Scientific Research Publishing

Energy and Power Engineering, 2026, 18(8), 521-556
https://www.scirp.org/journal/epe
ISSN Online: 1947-3818
ISSN Print: 1949-243X

Numerical Simulation and Experimental Investigation of Wall-Attached Air Retrofit for a 1000 MW Ultra-Supercritical Reverse Double Tangentially Fired Coal-Fired Boiler

Yong Feng[1], Zhidong Li[1], Jiahui Zhao[2], Zhenggang Wu[2], Weiyu Wang[3], Hanlin Li[3*]

[1]Hubei Chibi Electric Power Co., Ltd., Chibi, China
[2]Beijing Yelian Technology Co., Ltd., Beijing, China
[3]School of Energy Science and Engineering, Harbin Institute of Technology, Harbin, China
Email: *a1083698851@163.com

How to cite this paper: Feng, Y., Li, Z.D., Zhao, J.H., Wu, Z.G., Wang, W.Y. and Li, H.L. (2026) Numerical Simulation and Experimental Investigation of Wall-Attached Air Retrofit for a 1000 MW Ultra-Supercritical Reverse Double Tangentially Fired Coal-Fired Boiler. *Energy and Power Engineering*, **18**, 521-556.
https://doi.org/10.4236/epe.2026.188025

Received: July 25, 2026
Accepted: August 23, 2026
Published: August 26, 2026

Abstract

High-temperature corrosion of water-cooled walls is recognized as one of the major factors limiting the safe and stable operation of large coal-fired boilers. To address the high-temperature corrosion caused by the reducing atmosphere in the near-wall region of a 1000 MW ultra-supercritical reverse double tangentially fired coal-fired boiler, an optimized wall-attached air strategy is proposed. Numerical simulations and industrial tests are combined to investigate the effects of different wall-attached air fractions (2%, 3%, and 4%) on the temperature field and the distributions of O_2, CO, and H_2S in the near-wall region of the furnace. The results show that the combustion atmosphere adjacent to the water-cooled walls is improved after wall-attached air is introduced. The O_2 concentration is increased, whereas the CO and H_2S concentrations are reduced. However, the improvement is found to depend strongly on the wall-attached air fraction. At a wall-attached air fraction of 3%, the near-wall regions exhibit the highest O_2 concentrations and the lowest CO and H_2S concentrations among the investigated cases, and the lowest near-wall gas temperature are obtained, indicating the most favorable near-wall combustion environment. When the wall-attached air fraction is further increased to 4%, the improvement becomes less pronounced because of changes in the local combustion organization. The experimental results are found to be in good agreement with the numerical predictions. Under the 3% wall-attached air condition, the O_2 concentration in the high-temperature corrosion regions is increased to 2.15% - 19.90%, while the CO and H_2S concentrations are maintained within 0.01% - 3.51% and 0 - 518 ppm, respectively. The results demonstrate that an appropriate wall-attached air fraction improves the near-wall oxidizing atmosphere of a reverse double tangentially fired coal-fired boiler and suppresses the formation of reducing corrosive species, thereby mitigating the tendency for high-temperature corrosion of the water-cooled walls. The present study provides theoretical support and engineering guidance for the optimization of wall-attached air systems and the mitigation of water-cooled wall high-temperature corrosion in large tangentially fired coal-fired boilers.

Keywords

Reverse Double-Tangentially Fired Coal-Fired Boiler, High-Temperature Corrosion, Wall-Attached Air, Sensitivity Analysis

1. Introduction

Under the background of the continuous advancement of the "dual-carbon" strategy, the energy structure of China is accelerating its transition toward a low-carbon direction [1]. However, due to factors such as renewable energy accommodation capacity, power system peak regulation requirements, and energy security demands, coal-fired power units will continue to play an important role in ensuring safe and stable electricity supply for a relatively long period in the future [2] [3]. With the continuous increase in the installed capacity of renewable energy, the operation mode of coal-fired power units is gradually shifting from traditional base load operation to deep peak regulation and frequent load variation operation. The fluctuations of operating conditions have increased significantly, imposing higher requirements on the safety, stability, and long-term reliable operation capability of boiler equipment [4]. As the core thermal equipment of coal-fired power units, boilers operate under high-temperature, high-pressure, and complex chemical reaction environments for a long time. The performance degradation of heat-transfer surface materials is caused by the combined effects of combustion products and corrosive media [5]. Among these issues, high-temperature corrosion of water-cooled walls is one of the major problems affecting safe operation of boilers. Long-term corrosion can result in wall thinning and reduced pressure-bearing capacity, and may even cause leakage or tube burst accidents under severe conditions [6]. According to relevant studies, approximately 80% of coal-fired boilers suffer from different degrees of high-temperature corrosion of water-cooled walls [7], and about 35% of unplanned shutdown accidents are related to this problem [8]. This not only affects the safe operation of power units but also causes considerable economic losses.

High-temperature corrosion of water-cooled walls in coal-fired boilers mainly occurs in the form of sulfide-type corrosion, and its formation is closely related to the reducing atmosphere in the near-wall region of the furnace [9]. During the application of low-NO_X combustion technology, air-staged combustion is generally adopted to reduce NO_X formation, resulting in the formation of a certain reducing environment in the burner region [10]. When oxygen-deficient regions exist near the water-cooled wall, sulfur generated during pulverized coal combustion is easily converted into corrosive gases such as H_2S, which further react with the metal matrix to form sulfide corrosion products, accelerating the failure of water-cooled wall materials [11]. Studies have shown that the corrosion rate generally increases with increasing H_2S concentration, while increasing the oxygen concentration in the near-wall region can promote the oxidation of reducing gases and reduce H_2S formation, thereby improving the corrosion environment [12]. Therefore, regulating the atmospheric conditions near the water-cooled wall and reducing the concentration of reducing species are important approaches for preventing high-temperature corrosion.

Currently, various mitigation strategies have been proposed by researchers to address high-temperature corrosion of water-cooled walls in coal-fired boilers, including combustion optimization [13], development of corrosion-resistant water-cooled wall materials [14], surface protective coating techniques [15], and near-wall gas atmosphere regulation technologies [16]. Among these approaches, material modification and protective coatings can improve the corrosion resistance of water-cooled walls; however, they generally suffer from high costs and limitations in long-term operational reliability. Combustion optimization and air distribution adjustment can improve the overall combustion environment inside the furnace, but their ability to regulate localized corrosion-prone regions remains limited. Therefore, near-wall gas atmosphere regulation technology, which directly modifies the combustion atmosphere near the water-cooled wall, has gradually attracted increasing attention.

Jin *et al.* [17] investigated the high-temperature corrosion behavior of two representative water-cooled wall tube materials, 20 G and 12Cr1MoV, under oxy-fuel combustion conditions. The effects of temperature, elevated CO_2 concentration, water vapor, and reducing gases on corrosion behavior are systematically evaluated. The results show that elevated CO_2 concentration and water vapor in oxy-fuel flue gas increased the corrosion rate by 10% - 30%, while the reducing atmosphere promoted the formation of iron sulfide, thereby accelerating corrosion. Ning *et al.* [18] investigated the effects of boiler load, burner tilt angle, and the number of near-wall air nozzles on high-temperature corrosion of water-cooled walls in a 600 MW opposed-firing boiler. The results indicate that reducing the boiler load could decrease the wall temperature. However, the H_2S concentration did not show a monotonically decreasing trend. The adjustment of burner tilt angle has no significant effect on corrosion mitigation, whereas near-wall air could effectively improve the reducing atmosphere near the water-cooled wall and reduce corrosion risk. Liu *et al.* [19] investigated the effects of near-wall air arrangement location and air distribution ratio on high-temperature corrosion characteristics of boilers through numerical simulation. The results show that when the near-wall air ratio is 1%, the side-wall arrangement could significantly reduce CO and H_2S concentrations near the wall while maintaining favorable combustion performance. Liu *et al.* [20] developed a corrosion prediction model coupled with H_2S concentration and wall temperature for the high-temperature corrosion problem of water-cooled walls in a 660 MW boiler. Furthermore, the effects of different boiler load conditions and recirculated flue gas near-wall air (RFG-NWA) are investigated. The results indicate that protective measures are required when the boiler load exceeded 50% THA. The maximum corrosion depth is reduced by approximately 50% through the application of 7% RFG-NWA without compromising combustion stability, demonstrating the potential of near-wall atmosphere regulation technology for engineering corrosion protection. Wang *et al.* [21] proposed a secondary air distribution strategy for a 1000 MW ultra-supercritical reverse double tangentially fired boiler to improve the combustion environment in the cold corner region. The numerical results indicate that an appropriate increase in secondary air flow effectively suppresses high-temperature corrosion of the water-cooled walls. Yue *et al.* [22] effectively controlled high-temperature corrosion of water-cooled walls through comprehensive measures, including increasing operating oxygen concentration, optimizing air distribution, optimizing coal blending, and applying anti-corrosion coatings. Lv *et al.* [23] performed a numerical investigation of burner geometry and secondary air injection. The results show that a smaller burner aspect ratio and upward secondary air injection at 15˚ increase the oxygen concentration near the water-cooled wall. As a result, the local reducing atmosphere is weakened and high-temperature corrosion is mitigated.

Among the existing near-wall atmosphere regulation technologies, wall-attached air has attracted considerable attention for mitigating high-temperature corrosion. It offers a low retrofit cost, strong adaptability, and only a limited impact on overall boiler operation. This technology introduces a certain proportion of the primary or the secondary air into the near-wall region through nozzles installed near high-temperature corrosion-sensitive areas. The increased oxygen concentration promotes the oxidation of reducing species, such as CO and H_2S, thereby suppressing sulfide-type high-temperature corrosion.

Extensive studies on wall-attached air retrofit have been carried out for coal-fired boilers with different capacity levels. Liu *et al.* [24] arranged three layers of wall-attached air nozzles near the side-wall regions of the front and rear walls in a 600 MW supercritical opposed-firing boiler. The test results show that wall-attached air could significantly increase the oxygen concentration in the near-wall region and effectively weaken the reducing atmosphere inside the furnace. Cui *et al.* [25] installed four layers of wall-attached air nozzles on both side walls of a 670 MW supercritical opposed-firing boiler. After the retrofit, the reducing atmosphere inside the furnace is significantly weakened, and high-temperature corrosion of water-cooled walls is effectively suppressed. Chen *et al.* [26] investigated the influence of wall-attached air arrangement on the near-wall atmosphere of a 660 MW ultra-supercritical opposed-firing boiler through numerical simulation. The results indicate that when the wall-attached air ratio exceeded 3%, the oxygen volume fraction in the near-wall region of the side walls could be significantly increased, thereby improving the corrosion environment. Qiu *et al.* [27] installed 16 groups of wall-attached air nozzles on the front and rear walls of a 660 MW ultra-supercritical boiler. Field tests confirmed that the wall-attached air system increased the oxygen concentration near the water-cooled wall and alleviated high-temperature corrosion.

In summary, combustion optimization, air distribution adjustment, anti-corrosion coatings, and wall-attached air technology can reduce the risk of high-temperature corrosion of water-cooled walls to some extent. Among these methods, combustion optimization and material protection measures mainly work by improving the overall combustion conditions or enhancing the corrosion resistance of materials, but their ability to precisely regulate localized corrosion regions remains limited. In comparison, wall-attached air technology can directly improve the oxygen concentration distribution and flue gas composition near the water-cooled wall, reduce the concentrations of corrosive species such as CO and H_2S, and weaken the formation conditions of high-temperature corrosion at the source. Therefore, wall-attached air technology has good engineering application value and is considered one of the relatively economical and effective retrofit measures for preventing high-temperature corrosion of water-cooled walls. This technology generally introduces a certain amount of the primary air or the secondary air into the near-wall region of the furnace by arranging nozzles upstream of corrosion regions on the water-cooled wall or installing air injection devices directly in corrosion-prone wall areas. The introduced air increases the oxygen concentration in the corresponding region and weakens the local reducing atmosphere. This measure effectively disrupts the conditions required for high-temperature corrosion formation, thereby reducing the corrosion rate and extending the service life of water-cooled walls. However, existing studies on wall-attached air technology mainly focus on opposed-firing boilers, while investigations on tangentially fired boilers, especially reverse double tangentially fired boilers, remain relatively limited. Due to the complex swirling flow field in tangentially fired boilers, the airflow organization near the water-cooled wall, temperature distribution, and migration characteristics of corrosive gases are significantly different from those in opposed-firing boilers. Therefore, the regulation mechanism of wall-attached air on the near-wall atmosphere and the optimal operating parameters still requires further investigation.

Therefore, to address the high-temperature corrosion of water-cooled walls in reverse double tangentially fired boilers, a 1000 MW ultra-supercritical unit is selected as the study object. An optimized wall-attached air scheme is proposed based on previous studies of near-wall atmosphere regulation. Numerical simulations and industrial tests are conducted to investigate the effects of different wall-attached air parameters on the temperature field, flue gas composition, and combustion characteristics in the near-wall region of the furnace. The effectiveness of wall-attached air technology in improving the high-temperature corrosion environment of water-cooled walls is evaluated. A theoretical basis for the engineering application of wall-attached air technology in large-scale reverse double tangentially fired boilers is thus provided.

2. Methodology

2.1. Boiler Description

The investigated boiler is an HG-3101/27.46-YM3 ultra-supercritical variable-pressure once-through boiler installed in a power plant. The boiler adopts a Π-type configuration with a single furnace and a single-reheat system, and the furnace has a cross-sectional dimension of 34,220 mm × 15,670 mm. A low-NO_X combustion system incorporating low-NO_X burners and high-level over-fire air is employed, while reverse double-tangential firing is adopted as the combustion mode. The overall configuration of the boiler is illustrated in **Figure 1**.

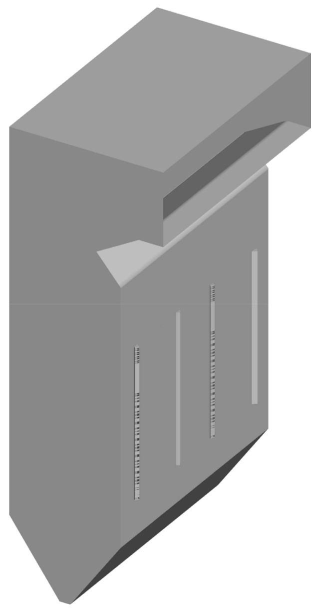

Figure 1. Overall structure schematic diagram of the furnace chamber.

The burner region adopts an octagonal double tangential firing configuration without partition walls, and fully tilting burners are employed. Six layers of pulverized coal nozzles are arranged along the furnace height, numbered from bottom to top as A-F. Each layer of pulverized coal nozzles corresponds to one pulverizer. In addition, three layers of oil air compartments and ten layers of auxiliary air compartments are arranged. The nozzles of each burner jointly form an imaginary tangential circle, as shown in **Figure 2**. Over the main burners, over-fire air nozzles are arranged. Meanwhile, four layers of additional over-fire air nozzles are installed at a distance of 7.2 m above the upper pulverized coal nozzles. The additional over-fire air nozzles supply supplemental air required for the combustion of unburned fuel components in the later combustion stage, promote further burnout of unburned species, and reduce the local temperature level in the furnace, thereby achieving staged combustion and suppressing NO_X formation.

During the scheduled outage, an on-site inspection and measurement of high-temperature corrosion on the furnace water walls are conducted. The results revealed that high-temperature corrosion is mainly concentrated in the #5 and #8 corners regions. Measurements indicated that the vertical extent of the corroded regions is nearly identical at both corners, extending from the uppermost F-layer primary air burner to the uppermost over-fire air level, with a total height of approximately 9 m. In the horizontal direction, the corroded regions originate from the corner water walls and extend toward the adjacent walls. The corrosion-affected width is approximately 5 m along both the left and right water walls and 4 m along the rear water wall. The distribution of the high-temperature corrosion regions inside the furnace is illustrated in Figure 3.

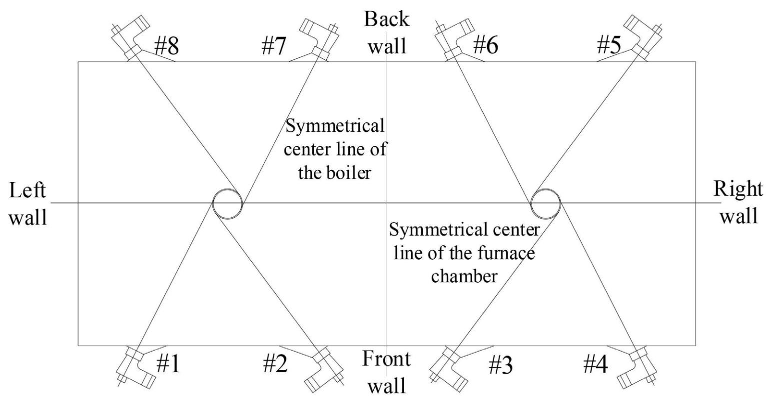

Figure 2. Hypothetical circular section of the furnace chamber.

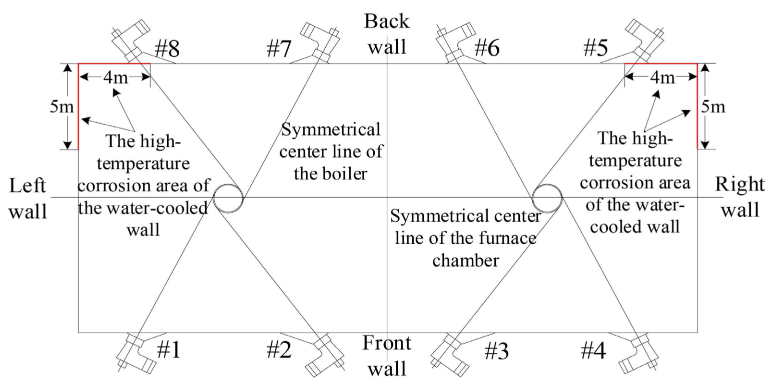

Figure 3. Plan view of the high-temperature corrosion area within the furnace.

2.2. Experimental Investigation

High-temperature corrosion of water walls is closely associated with the reducing atmosphere and the concentration of corrosive H_2S near the wall surface. To characterize the near-wall atmosphere in the burner region and clarify its distribution under different operating conditions, near-wall atmosphere measurements and operational adjustment tests are conducted. The boiler is operated at a stable load of 1000 MW during the experiments. Three operating conditions are investigated, including the baseline test, oxygen level adjustment test, and air distribution adjustment test. The baseline test is performed to characterize the near-wall atmosphere under the original operating condition. The oxygen level adjustment test is conducted by varying the furnace oxygen level to evaluate the influence of the excess air ratio on the near-wall atmosphere. The air distribution adjustment test is carried out by modifying the burner air distribution to investigate the variation in the near-wall flue gas composition under different air distribution conditions.

1) Baseline test

Before conducting the oxygen level adjustment and air distribution adjustment tests, baseline measurements of the near-wall atmosphere under the conventional operating condition are first performed to characterize the atmospheric conditions in the burner region.

Figure 4 presents the near-wall atmosphere measured under the baseline operating condition. The boiler is operated at a furnace outlet oxygen concentration of 2.2%.

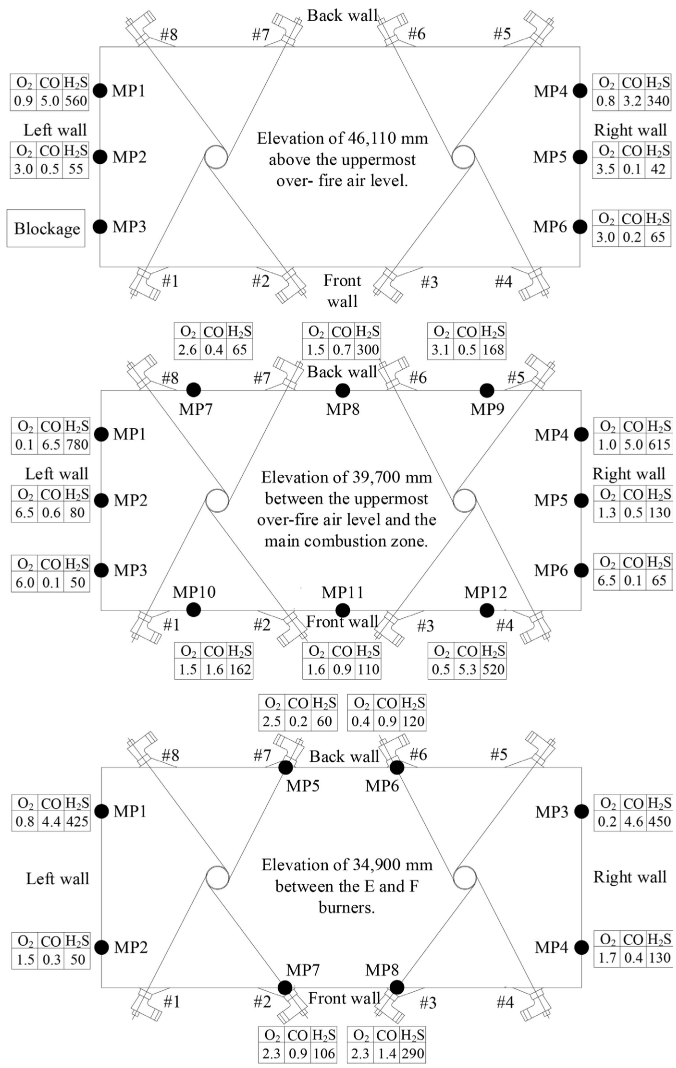

Figure 4. Test results of near-wall atmosphere in the burner region under the baseline test condition.

As shown in **Figure 4**, strong reducing atmospheres are observed at measurement point 1 near burner #8 on the left water wall and measurement point 4 near burner #5 on the right water wall at elevations of 39,700 and 46,110 mm. The O_2 concentration ranges from 0.1% to 1.0%, whereas the CO and H_2S concentrations range from 3.2% to 6.5% and 340 to 780 ppm, respectively. At an elevation of 34,900 mm, a pronounced reducing atmosphere is also observed at measurement point 1 near burner #8 on the left water wall and Measurement Point 3 near Burner #5 on the right water wall. The corresponding O_2, CO, and H_2S concentrations are 0.2% - 0.8%, 4.4% - 4.6%, and 425 - 450 ppm, respectively. The measurements consistently indicate a typical low-O_2, high-CO, and high-H_2S atmosphere near the water walls in the burner regions of corners #5 and #8.

2) Oxygen level adjustment test

The furnace outlet oxygen concentration is increased from 2.2% to 2.5% - 3.0% based on the baseline operating condition. Slight fluctuations in the actual oxygen concentration are observed during the test. The measured near-wall atmosphere under the oxygen level adjustment condition is presented in **Figure 5**. The atmosphere distribution remains generally consistent with that observed under the baseline condition. At elevations of 39,700 and 46,110 mm, measurement point 1 near

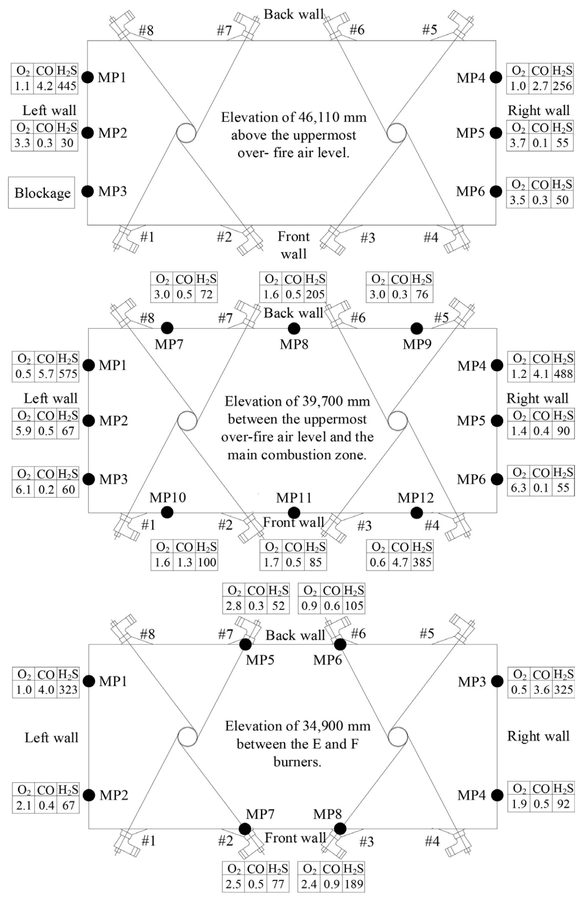

Figure 5. Measurement results of the near-wall atmosphere in the burner region under the oxygen adjustment test.

burner #8 on the left water wall and measurement point 4 near burner #5 on the right water wall still exhibit a pronounced reducing atmosphere with relatively high H_2S concentrations. The corresponding O_2, CO, and H_2S concentrations range from 0.5% to 1.2%, 2.7% to 5.7%, and 256 to 575 ppm, respectively. Compared with the baseline condition, increasing the furnace outlet oxygen concentration increases the O_2 concentration while reducing the CO and H_2S concentrations near the water walls in the #5 and #8 corners regions.

3) Air distribution adjustment test

The furnace outlet oxygen concentration is maintained at 2.5%, and the air distribution is further optimized. To weaken the strongly reducing atmosphere, +20% bias is applied to the rear secondary air dampers on both the left and right water walls, thereby increasing the damper opening from 40% to 60% and enhancing the secondary air supply to the affected regions.

Figure 6 presents the measured near-wall atmosphere in the burner region under the air distribution adjustment condition. As shown in **Figure 6**, the near-wall atmosphere at the elevations of 39,700 mm and 46,110 mm exhibited distribution characteristics similar to those observed in the previous two tests. Measurement point 1 near burner #8 on the left water wall and measurement point 4 near burner #5 on the right water wall remained the regions with the strongest reducing

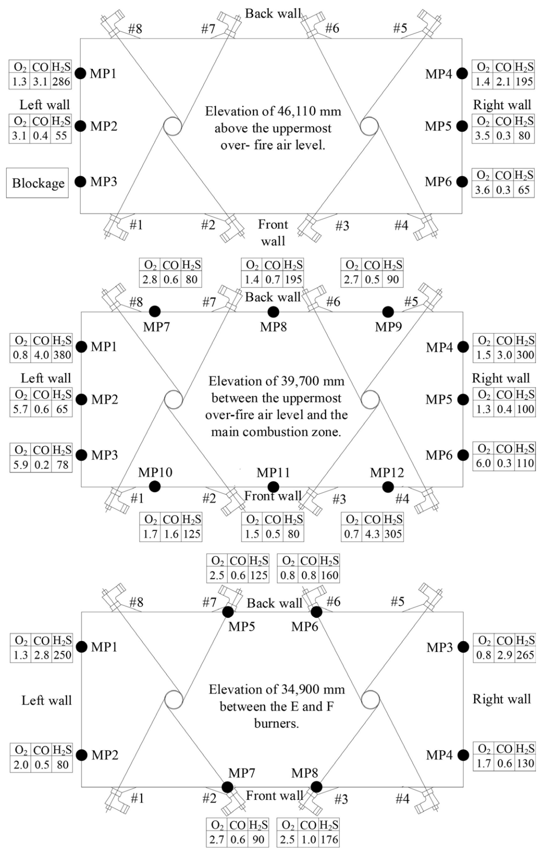

Figure 6. Near-Wall atmosphere measurement results in the burner region under the air distribution adjustment condition.

atmosphere. The measured O_2, CO, and H_2S concentrations ranged from 0.8% to 1.5%, 2.1% to 4.0%, and 195 to 380 ppm, respectively. Compared with the previous two tests, the O_2 concentration in the #5 and #8 corners regions changed only slightly after the air distribution adjustment, whereas the CO and H_2S concentrations decreased further.

The measurement results of the near-wall atmosphere in the burner region lead to the following conclusions:

1) Under the baseline operating condition, the near-wall atmosphere in the burner region generally follows the rotation direction of the tangential firing circle. Reducing atmospheres are observed on the fire-facing sides of all four furnace corners, with the strongest reducing atmosphere occurring near the side walls in the #5 and #8 corners regions. The O_2 concentration is approximately 0.6%, while the CO concentration is about 5% and the H_2S concentration ranges from 400 to 700 ppm. These conditions favor the occurrence of high-temperature corrosion.

2) After the operating oxygen level is increased and the air distribution is optimized, the O_2 concentration in the #5 and #8 corners regions increases, whereas the CO and H_2S concentrations decrease. This indicates that the local reducing atmosphere is alleviated. Under the optimized operating condition, the O_2 concentration is approximately 1.2%, while the CO and H_2S concentrations decrease to 2% - 4% and 200 - 400 ppm, respectively. However, relatively high concentrations of reducing gases are still observed, suggesting that the conditions for high-temperature corrosion are not completely eliminated.

3) The results obtained under all three operating conditions consistently show that the strongest reducing atmosphere occurs in the near-wall regions of corners #5 and #8. The locations of these reducing atmosphere zones remain essentially unchanged under different operating conditions and agree well with the high-temperature corrosion regions identified during the field inspection.

2.3. Improvement Strategy

To mitigate high-temperature corrosion of water-cooled walls in coal-fired boilers, a novel wall-attached air technology is proposed to directly introduce additional air into the corrosion-prone regions and improve the near-wall combustion environment. A numerical sensitivity analysis is conducted to evaluate the effect of the wall-attached air fraction on the near-wall combustion characteristics. The wall-attached air fraction is selected as the key variable, whereas the furnace geometry, burner operating conditions, and other boundary conditions are kept unchanged. Three simulation cases with wall-attached air fractions of 2%, 3%, and 4% are established. The corresponding temperature field, near-wall oxygen distribution, and the concentrations of CO and H_2S are compared. Finally, the effects of different air fractions on the high-temperature corrosion tendency of the water-cooled walls are evaluated (**Figure 7**).

To ensure a consistent comparison among different simulation cases, the locations and geometric configurations of the wall-attached air nozzles are kept identical. Four columns of nozzles are arranged in the high-temperature corrosion regions at corners #5 and #8. Three columns are symmetrically installed on the left and right water walls, whereas one column is arranged on the rear water wall adjacent to each side wall. Along the furnace height, eight nozzle layers are installed between the elevation of 34,000 mm below the F-layer burners and the elevation of 44,500 mm above the uppermost over-fire air level, with a vertical spacing of 1500 mm. A total of 64 nozzles are employed in the present study.

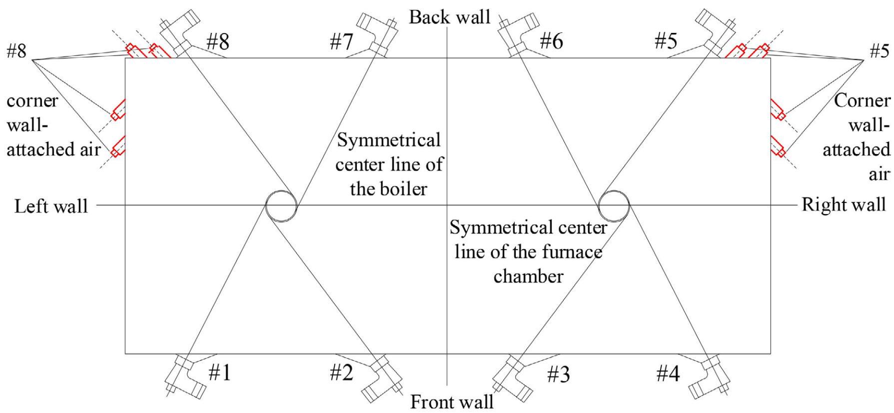

Figure 7. Schematic diagram of the wall-attached air arrangement scheme.

In the numerical simulations, wall-attached air is extracted from the secondary air boxes on the front and rear walls and introduced into the furnace through independent air ducts connected to each nozzle. To ensure the comparability of the simulation results, the boiler geometry, burner operating parameters, and boundary conditions are kept unchanged for all cases. Only the ratio of the total wall-attached air flow rate to the total furnace air flow rate is varied. Three wall-attached air fractions of 2%, 3%, and 4% are considered. The temperature field and the distributions of O_2, CO, and H_2S in the near-wall region are analyzed under each operating condition, and the optimum wall-attached air fraction for the reverse double tangentially fired coal-fired boiler is determined.

3. Numerical Model

3.1. Boundary Conditions

A three-dimensional computational model extending from the boiler hopper to the reheater outlet is established using GAMBIT. The model is constructed at full scale based on the actual boiler dimensions, whereas non-critical structural details are simplified to improve computational efficiency. According to the flow characteristics in the furnace and the pulverized coal combustion process, the computational domain is divided into four regions along the furnace height, namely the hopper region, the main combustion region, the burnout region, and the horizontal flue region. The computational mesh is generated separately for each region according to its geometric characteristics. The final three-dimensional computational mesh is shown in **Figure 8**.

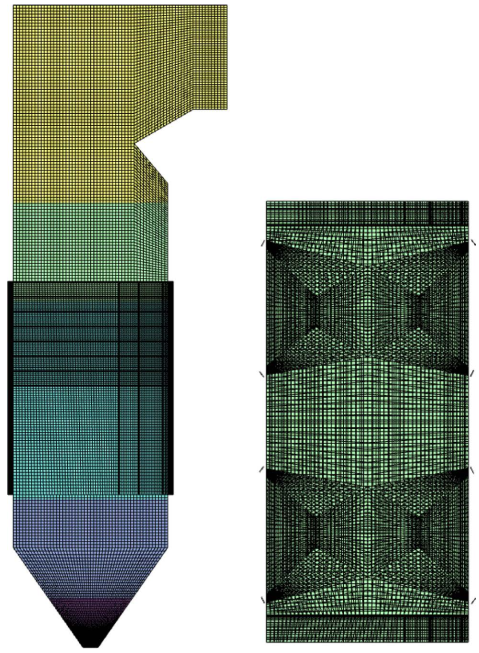

Figure 8. Three-dimensional computational mesh.

In this study, the furnace outlet refers to the outlet cross-section of the three-dimensional computational model. In the computational domain, the water-cooled walls, burner nozzles, and heat-transfer surfaces are treated as zero-thickness walls to simplify the model. To improve the prediction accuracy in the main combustion region, local mesh refinement is applied in this region. An O-grid structure is adopted to align the mesh with the flow direction, thereby reducing numerical diffusion during the simulation.

To account for the actual heat transfer characteristics of the furnace water walls, no-slip velocity and fixed wall temperature boundary conditions are imposed on the furnace walls. The main operating parameters of the boiler under the 1000 MW load condition are listed in **Table 1**. During the simulations, the properties of pulverized coal and the coal quality are specified according to the design coal, and the corresponding proximate and ultimate analyses are presented in **Table 2**.

The Semi-Implicit Method for Pressure Linked Equations algorithm is employed to handle the coupling between the pressure and velocity fields. During the solution process, the velocity and pressure fields are initially assumed, and the pressure field is subsequently corrected based on the calculated velocity field to satisfy mass conservation. To describe the complex turbulent flow generated by the interaction of high-velocity jets and swirling flow in the furnace, the Realizable k-ε turbulence model is adopted. Compared with the standard k-ε model, the Realizable k-ε model provides more accurate predictions of swirling, separated, and strongly sheared flows [28]. The gas-solid two-phase flow is described using the Euler-Lagrange approach. The continuous gas phase is solved in the Eulerian framework, whereas the discrete pulverized coal particles are tracked in the lagrangian framework. The influence of turbulent fluctuations on particle motion is taken into account using the Discrete Random Walk model, which describes the interaction between particles and turbulent eddies [29]. Mass, momentum, and energy exchanges between the gas and particle phases are coupled through the Cell Source Method, in which the effects of the discrete particle phase on the continuous phase are incorporated into the governing equations as source terms.

Radiative heat transfer within the furnace is calculated using the P-1 radiation model. By solving the first-order approximation of the radiative transfer equation, the P-1 model provides a reasonable balance between computational accuracy and efficiency and is widely applied to radiative heat transfer simulations in large-scale industrial furnaces [30].

Table 1. Design parameters under stable 1000 MW load conditions.

Parameter	Base case	Retrofitted Condition
Coal consumption ($t \cdot h^{-1}$)	378.47	
Total air flow rate ($t \cdot h^{-1}$)	3360.57	
Number of operating mills	5.00	
The primary air ratio (%)	28.49	
Air leakage ratio (%)	5.00	
Furnace outlet O_2 concentration (%)	2.62	
The secondary air ratio (%)	65.51	62.51
Wall-attached air fraction (%)	/	3%

Table 2. Proximate and ultimate analysis of coal.

Parameters	Value
Carbon (as received basis, %)	60.33
Hydrogen (as received basis, %)	3.62
Oxygen (as received basis, %)	9.94
Nitrogen (as received basis, %)	0.70
Total sulfur (as received basis, %)	0.41
Total moisture (%)	14.00
Ash (as received basis, %)	11.00
Volatile matter (dry ash-free basis, %)	36.50
Lower heating value (as received basis, MJ/kg)	22.76

The pulverized coal combustion process is divided into three stages, including volatile release, volatile combustion, and char combustion. The volatile release process is described using the Two-Step Competitive Reaction Model, which accounts for the competing reaction pathways of volatile species during coal pyrolysis and improves the prediction accuracy of volatile release [31]. Volatile combustion is simulated using the Eddy Dissipation Model, in which the reaction rate is assumed to be controlled primarily by the turbulent mixing rate, making the model suitable for industrial combustion simulations [32]. The char combustion process is described using the Kinetic/Diffusion Model, which simultaneously considers the surface reaction kinetics of char and the diffusion resistance of oxygen to the particle surface, thereby improving the reliability of char burnout predictions [33].

3.2. Model

To accurately describe the complex processes of gas flow, heat transfer, and species transport during pulverized coal combustion, the continuous medium assumption is adopted in this study. The gas phase inside the furnace is treated as a compressible continuous fluid, and its flow behavior is governed by the conservation equations of mass, momentum, and energy.

The mathematical expression of the mass conservation equation describing the pulverized coal flow is given as follow [16]:

$$\frac{\partial \rho}{\partial t}+\frac{\partial}{\partial x_i}\left(\rho u_i\right)=0 \tag{1}$$

The mathematical expression of the energy conservation equation describing the pulverized coal flow is given as follows [26]:

$$\frac{\partial}{\partial t}(\rho h)+\frac{\partial}{\partial x_i}\left(\rho u_j h\right)=-p\frac{\partial u_j}{\partial x_j}+\frac{\partial}{\partial x_j}\left(\lambda\frac{\partial T}{\partial x_j}\right)+\Phi+S_h \tag{2}$$

where $\frac{\partial}{\partial x_j}\left(\lambda\frac{\partial T}{\partial x_j}\right)$ represents the thermal conductivity of pulverized coal per unit volume; Φ represents the mechanical energy dissipation during the flow process; S_h represents the volumetric heat sources.

The momentum conservation equation governing the pulverized coal flow is given as follows [16]:

$$\frac{\partial}{\partial t}(\rho h)+\frac{\partial}{\partial x_i}\left(\rho u_j h\right)=-\frac{\partial \sigma_{ij}}{\partial x_j}+S_i \tag{3}$$

$$\sigma_{ij}=p\delta_{ij}-\tau_{ij},\quad \tau_{ij}=\mu\left(\frac{\partial u_i}{\partial x_j}+\frac{\partial u_j}{\partial x_i}\right)-\frac{2}{3}\mu\frac{\partial u_i}{\partial x_i}\delta_{ij},\quad \delta_{ij}=\begin{cases}0 & i\neq j\\ 1 & i=j\end{cases}.$$

To predict the H_2S concentration distribution near the water-cooled wall region during coal combustion, the Coal Combustion model coupled with the built-in SO_X model in Fluent is employed to simulate the release and transformation of sulfur-containing species. The SO_X model is based on the default simplified global sulfur reaction mechanism provided by Fluent, which describes the release of fuel sulfur during volatile matter evolution and char combustion, as well as the subsequent conversion among gas-phase sulfur species. The reaction pathways, rate constants, and related kinetic parameters are adopted from the predefined Fluent database and automatically invoked during the simulation.

During coal combustion, sulfur contained in coal is mainly released into the gas phase through volatile matter evolution and char combustion, followed by gas-phase sulfur transformation reactions. The major sulfur-containing gas species considered in the SO_X model include H_2S, SO_2, COS, and CS_2. The conversion among sulfur species is strongly influenced by local temperature, oxygen concentration, and reducing atmosphere conditions in the furnace. Among these sulfur species, H_2S is regarded as an important indicator for characterizing the reducing environment near the water-cooled wall region and evaluating the potential risk of sulfur-related corrosion. In this study, the default reaction mechanism and kinetic parameters embedded in the Fluent SO_X model are directly adopted for the simulations.

The representative sulfur species conversion pathways involved in the SO_X model are described as follows:

$$SO_2 + 3H_2 \rightarrow H_2S + 2H_2O \tag{4}$$

$$H_2S + \frac{3}{2}O_2 \rightarrow SO_2 + H_2O \tag{5}$$

$$SO_2 + CO + H_2O \rightarrow COS + H_2O \tag{6}$$

$$COS + H_2O \rightarrow H_2S + CO_2 \tag{7}$$

$$CS_2 + H_2O \rightarrow H_2S + COS \tag{8}$$

The above reaction pathways collectively describe the migration and transformation processes of sulfur species under reducing and oxidizing environments during coal combustion.

3.3. Model Validation

To validate the reliability of the established mathematical model, the simulated gas compositions are compared with the field-measured results. First, the furnace outlet O_2 concentration under the oxygen adjustment test condition is compared with the measured value to verify the overall combustion condition of the boiler. In addition, considering that high-temperature corrosion is mainly associated with the near-wall reducing atmosphere, the simulated near-wall O_2, CO, and H_2S concentrations at individual measurement points in the corrosion-sensitive regions are further compared with the field measurements.

The comparison results are presented in **Table 3**. The simulated furnace outlet O_2 concentration agrees well with the measured value, with a relative error of 4.96%. Meanwhile, the simulated near-wall O_2, CO, and H_2S concentrations show good agreement with the measured values at different locations. The maximum relative errors of the predicted species concentrations are all within 10%, indicating that the developed numerical model can reasonably reproduce the near-wall combustion atmosphere and sulfur-containing species distribution in the high-temperature corrosion regions.

To verify the reliability of the numerical results, three computational meshes containing 3.58 million, 4.35 million, and 5.36 million cells are established. The

CO concentration distribution along the furnace height from 0 to 45 m at a location 9 m away from the left wall is selected for the mesh independence analysis. The default convergence criteria of Fluent are adopted during the solution process. The default convergence criteria of Fluent are adopted.

Table 3. Validation of simulated O_2, CO, and H_2S concentrations at individual near-wall measurement points.

Parameters		Experimental value		Simulated value		Relative error (%)		
Furnace outlet O_2 concentration (%)		2.62		2.75		4.96		
Elevation (mm)	Point	O_2 (%)		CO (%)		H_2S (ppm)		Maximum error (%)
		Exp.	Sim.	Exp.	Sim.	Exp.	Sim.	/
46,110	Point 1	1.1	1.2	4.2	4.4	445	475	9.09
	Point 2	3.3	3.5	0.3	0.3	30	32	6.67
	Point 3	\	\	\	\	\	\	\
	Point 4	1.0	1.0	2.7	2.8	256	275	7.42
	Point 5	3.7	4.0	0.1	0.1	55	59	8.11
	Point 6	3.5	3.8	0.3	0.3	50	52	8.57
39,700	Point 1	0.5	0.5	5.7	6.2	575	610	8.77
	Point 2	5.9	6.3	0.5	0.5	67	72	7.46
	Point 3	6.1	6.5	0.2	0.2	60	65	8.33
	Point 4	1.2	1.3	4.1	4.5	488	520	9.76
	Point 5	1.4	1.5	0.4	0.4	90	95	7.14
	Point 6	6.3	6.6	0.1	0.1	55	60	9.09
	Point 7	3.0	3.3	0.5	0.5	72	77	10.00
	Point 8	1.6	1.7	0.5	0.5	205	223	8.78
	Point 9	3.0	3.2	0.3	0.3	76	82	7.89
	Point 10	1.6	1.7	1.3	1.4	100	105	7.69
	Point 11	1.7	1.8	0.5	0.5	85	91	7.06
	Point 12	0.6	0.6	4.7	5.1	385	397	8.51

As shown in **Figure 9**, the variation trends of CO concentration along the furnace height are generally consistent under the three mesh resolutions. However, in the height range of 25 - 35 m, certain differences are observed among the results obtained with different mesh numbers. With increasing mesh resolution, the CO concentration distributions gradually became stable. Considering the accuracy requirements of the model, the mesh containing 5.36 million cells is finally selected for subsequent simulations.

4. Sensitivity Analysis

Under the 1000 MW load condition, the total furnace air flow rate remains

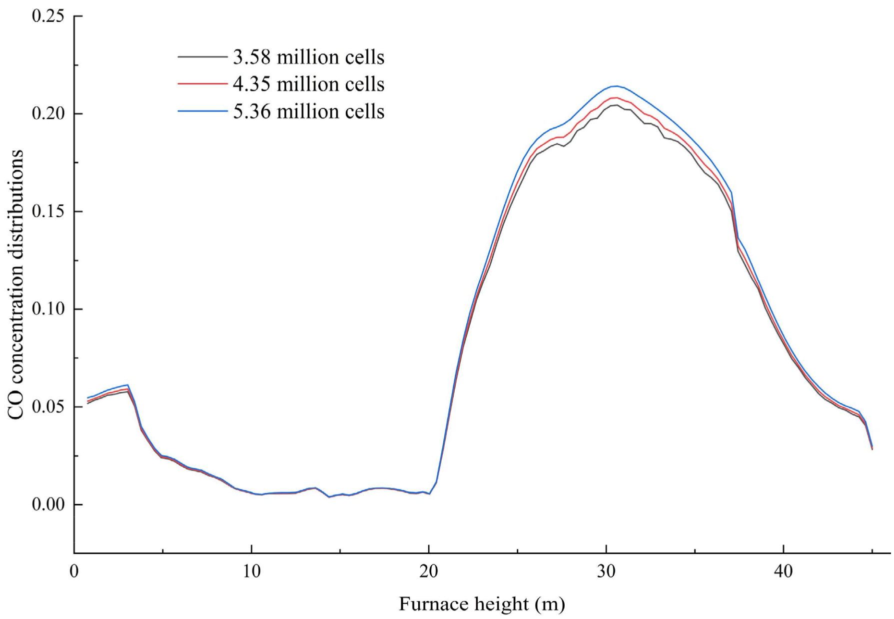

Figure 9. Mesh independence verification.

constant at 3360.57 t·h^{-1}. According to the designed wall-attached air ratios, the wall-attached air flow rates for the 2%, 3%, and 4% cases are 67.21 t·h^{-1}, 100.82 t·h^{-1}, and 134.42 t·h^{-1}, respectively. Since the wall-attached air is supplied by diverting a portion of the secondary-air flow, the increase in wall-attached air flow rate is compensated by an equivalent reduction in conventional secondary air flow rate, ensuring that the fuel input and total furnace air supply remain unchanged for all simulated cases. The wall-attached air ratios and corresponding air flow distributions under different conditions are listed in Table 4.

Table 4. Air mass flow rates under different wall-attached air ratios.

Case	Wall-attached air ratio (%)	Total furnace air flow rate (t·h^{-1})	Wall-attached air flow rate (t·h^{-1})	Secondary air flow rate (t·h^{-1})
Case 1	2%	3360.57	67.21	3293.36
Case 2	3%	3360.57	100.82	3259.75
Case 3	4%	3360.57	134.42	3226.15

4.1. Effect of Wall-Attached Air Fraction on Near-Wall Gas Temperature in High-Temperature Corrosion Regions of the Left, Right, and Rear Furnace Walls

Figure 10 shows the temperature distributions on the central cross-section of the F-layer burner under wall-attached air fractions of 2%, 3%, and 4%. As shown in the figure, the temperature fields exhibit an overall symmetrical distribution under different wall-attached air fractions, indicating that each burner can independently organize combustion and maintain the double-tangential firing characteristics. The pulverized coal can be sufficiently combusted, and no significant influence on the overall combustion process is observed after the installation of wall-attached air. Meanwhile, under different wall-attached air fractions, the high-temperature regions (1500 - 2000 K) remain mainly concentrated around the burners. The temperature field is relatively uniform without large-scale temperature deviations, demonstrating that the established model can reasonably represent the actual combustion conditions of the burners.

A comparison of the temperature distributions on the central cross-section of the F-layer burner under wall-attached air fractions of 2% (**Figure 10(a)**), 3% (**Figure 10(b)**), and 4% (**Figure 10(c)**) shows that the near-wall gas temperature at corners #5 and #8 decreases initially and then increases as the wall-attached air fraction increases. When the fraction increases from 2% to 3%, the near-wall gas temperature decreases markedly. This behavior is attributed to the modification of the near-wall flow field induced by the wall-attached air. The relatively low-temperature wall-attached air mixes with the high-temperature flue gas near the wall, enhancing the cooling effect of the near-wall gas region and reducing the gas temperature in the vicinity of the water-cooled wall. The introduced air enhances the mixing between the near-wall gas and the high-temperature flue gas, thereby improving the near-wall combustion environment. Meanwhile, the additional air entering the burner outlet region dilutes the high-temperature combustion zone and suppresses the local combustion intensity near the wall. Consequently, the near-wall gas temperature near corners #5 and #8 is reduced at a wall-attached air fraction of 3%, which is beneficial for mitigating high-temperature corrosion.

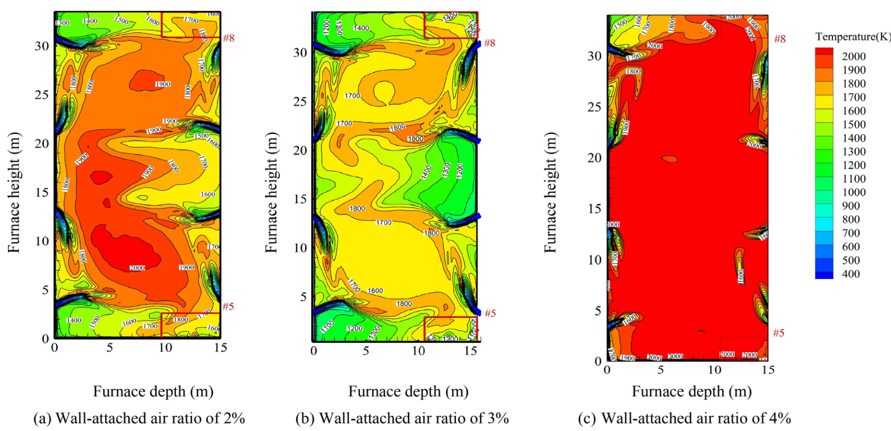

Figure 10. Temperature contours at the central plane of the F-layer burner with different wall-attached air fractions.

However, when the wall-attached air fraction is further increased to 4%, the near-wall gas temperature increases instead of continuing to decrease. This result suggests that excessive wall-attached air no longer further reduces the near-wall gas temperature because the combustion organization is altered. The increased air supply enhances the oxygen concentration near the wall and promotes the oxidation of incompletely burned combustible species, resulting in additional local heat release. Consequently, although more cooling air is introduced at a wall-attached air fraction of 4%, the enhanced combustion offsets the cooling effect, and no further reduction in the near-wall gas temperature is achieved.

Overall, a wall-attached air fraction of 3% provides the best balance among near-wall gas cooling, oxygen supply, and combustion stability. Under this condition, the lowest near-wall gas temperature is obtained near corners #5 and #8, thereby mitigating the high-temperature corrosion environment.

Figure 11 presents the temperature distribution along the height of the left furnace wall under different wall-attached air fractions. The wall-attached air fraction markedly affects the near-wall temperature, which decreases initially and then increases as the air fraction increases. At a wall-attached air fraction of 2% (Figure 11(a)), the cooling capacity of the wall-attached air is limited because of the relatively low air supply. Consequently, the high-temperature flue gas near the wall is not effectively cooled, and the thermal radiation from the flame and flue gas to the water-cooled wall remains strong. As a result, the near-wall gas temperature in the #8 high-temperature corrosion region exceeds 1500 K., indicating a high risk of high-temperature corrosion. As the wall-attached air fraction increases to 3% (Figure 11(b)), the temperature near the #8 corner decreases significantly, reaching approximately 1050 - 1300 K. This is mainly attributed to the enhanced coverage of the near-wall region by the cooling air with an appropriate increase in wall-attached air flow rate. The introduced air can effectively exchange heat with the high-temperature flue gas, thereby reducing heat accumulation near the furnace wall.

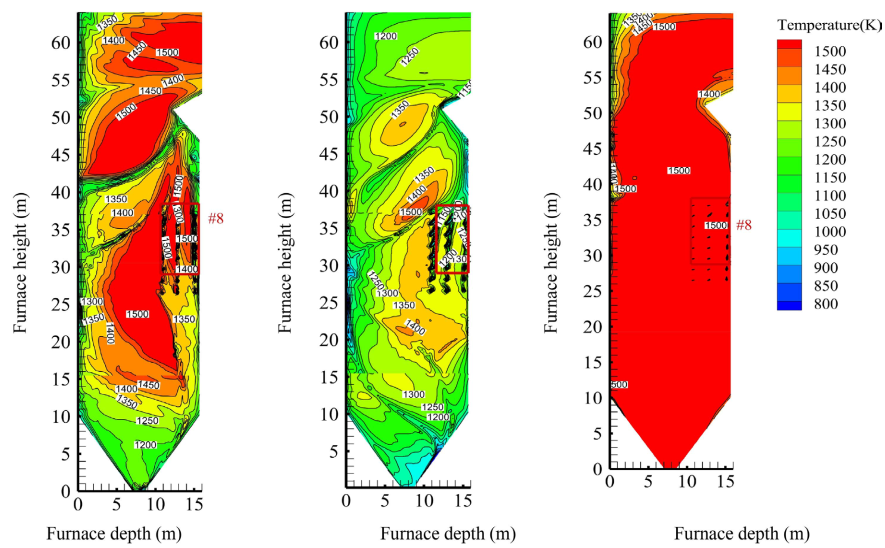

(a) Wall-attached air ratio of 2% (b) Wall-attached air ratio of 3% (c) Wall-attached air ratio of 4%

Figure 11. Temperature distributions on the left walls with different wall-attached air fractions.

However, when the wall-attached air fraction is further increased to 4% (Figure 11(c)), the overall furnace temperature rises markedly, accompanied by an expansion of the high-temperature region, with temperature exceeding 1500 K. This result indicates that further increasing the wall-attached air fraction does not improve the mitigation of high-temperature corrosion. Excessive wall-attached air increases the local oxygen concentration near the wall, thereby promoting the oxidation of unburned combustible species and increasing local heat release. As a result, the gas temperature in the furnace increases locally. In addition, the stronger wall-attached air jet disturbs the original flow field, causing the high-temperature flame zone to shift toward the furnace wall and increasing the near-wall gas temperature. Overall, a wall-attached air fraction of 3% reduces both the local and average near-wall gas temperature near the left furnace wall, providing the most favorable condition for mitigating high-temperature corrosion.

Figure 12 presents the temperature distribution along the height of the right furnace wall under different wall-attached air fractions. The near-wall gas temperature in the high-temperature corrosion region of the right furnace wall decreases initially and then increases as the wall-attached air fraction increases. At the wall-attached air fraction of 2% (Figure 12(a)), the cooling effect near the wall is limited because of the relatively low wall-attached air supply. As a result, the high-temperature flue gas is not effectively cooled, and the near-wall gas temperature near corner #5 remains within the range of 1400 - 1500 K, indicating a high risk of high-temperature corrosion.

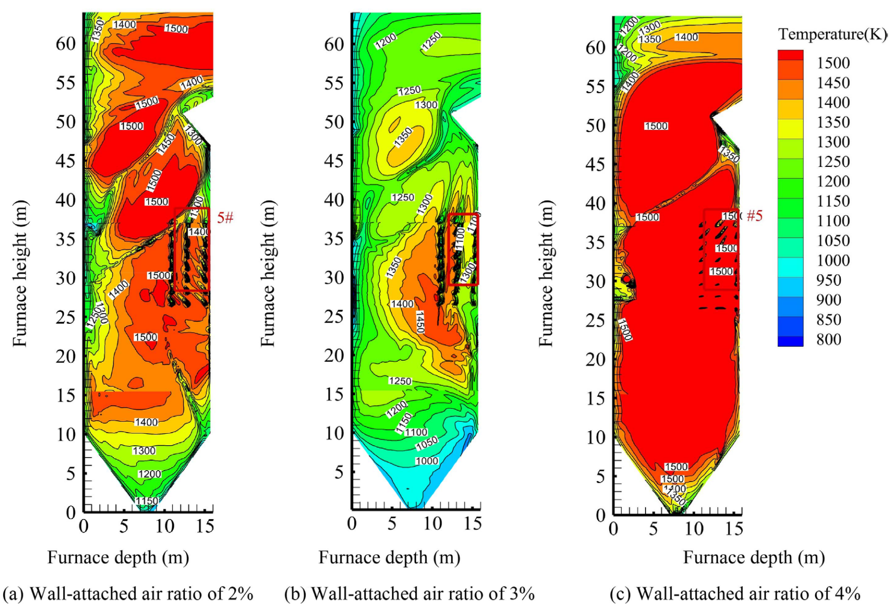

Figure 12. Temperature distributions on the right walls with different wall-attached air fractions.

When the wall-attached air fraction is increased to 3% (Figure 12(b)), the near-wall gas temperature near corner #5 decreases markedly to approximately 1100 - 1300 K, indicating that an appropriate wall-attached air supply effectively improve the near-wall gas temperature distribution. This reduction is attributed to the enhanced convective heat transfer induced by the wall-attached air, which weakens the heating effect of the high-temperature flue gas on the water-cooled wall. Consequently, heat accumulation near the wall is reduced, resulting in a lower local temperature and a less severe high-temperature corrosion environment.

However, when the wall-attached air fraction is further increased to 4% (**Figure 12(c)**), the near-wall gas temperature near corner #5 does not continue to decrease but instead rises, with the temperature exceeding 1500 K. This result suggests that excessive wall-attached air alters the oxygen distribution in the furnace. The additional oxygen enhances pulverized coal combustion and increases the overall heat release rate, leading to a higher furnace temperature. Although the wall-attached air provides a cooling effect, it is insufficient to compensate for the increased heat release caused by intensified combustion. Consequently, the near-wall gas temperature in the high-temperature corrosion region increases under the 4% wall-attached air fraction. Overall, a wall-attached air fraction of 3% provides the best balance between near-wall gas temperature regulation, oxygen supply, and combustion stability. Under this condition, the lowest near-wall gas temperature is obtained in the high-temperature corrosion region near corner #5 of the right furnace wall, providing the most favorable near-wall combustion environment for reducing the formation tendency of high-temperature corrosion.

Figure 13 presents the temperature distribution along the height of the rear furnace wall under different wall-attached air fractions. The near-wall gas temperature in the high-temperature corrosion region decreases initially and then increases as the wall-attached air fraction increases. Among all cases, the lowest near-wall gas temperature is obtained at a wall-attached air fraction of 3%, indicating that this condition is the most effective in mitigating high-temperature corrosion.

When the wall-attached air fraction is 2% (**Figure 13(a)**), the cooling effect in the near-wall region of the rear wall is limited because of the relatively low wall-attached air supply. As a result, the near-wall gas temperature near corners #5 and #8 remain within the range of 1400 - 1500 K, indicating that a 2% wall-attached air fraction is insufficient to effectively improve the thermal environment in the rear-wall high-temperature corrosion region.

When the wall-attached air fraction is increased to 3% (**Figure 13(b)**), the near-wall gas temperature near corners #5 and #8 decrease markedly to approximately 1050 - 1250 K. This reduction is attributed to the enhanced heat exchange between the introduced air and the high-temperature flue gas. In addition, the wall-attached air forms a relatively low-temperature air layer near the rear wall, which further weakens heat accumulation in the near-wall gas region. Consequently, the 3% wall-attached air fraction provides the most effective temperature control while maintaining stable combustion.

However, when the wall-attached air fraction is further increased to 4% (**Figure 13(c)**), the near-wall gas temperature near corners #5 and #8 rise again and exceed 1500 K. This result suggests that excessive wall-attached air no longer improves

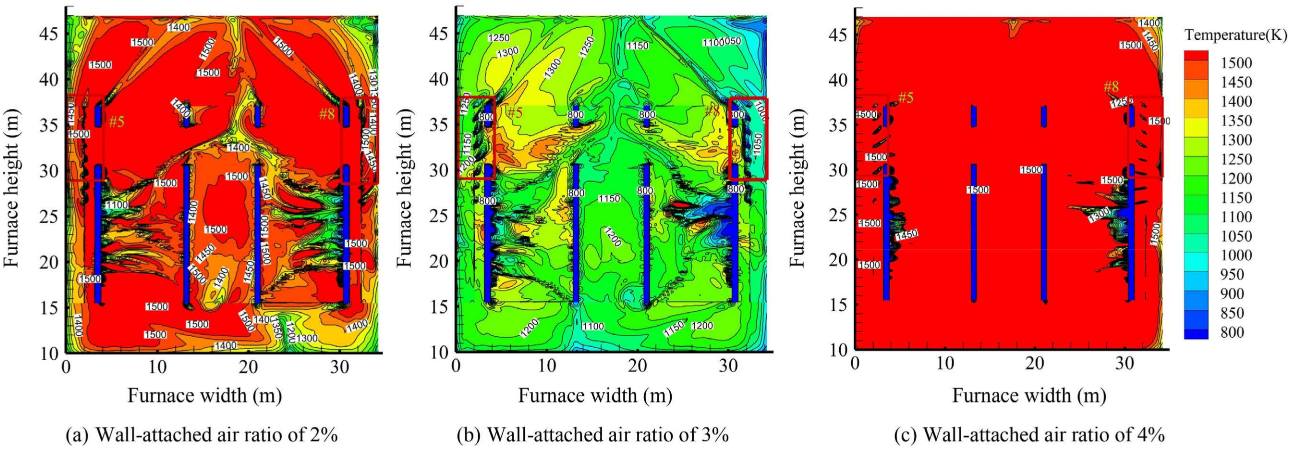

Figure 13. Temperature distributions on the rear walls with different wall-attached air fractions.

the near-wall thermal environment near the rear wall. The additional oxygen enhances pulverized coal combustion and increases the combustion intensity, leading to a higher furnace gas temperature. Although more cooling air is introduced, its cooling effect is offset by the intensified combustion. Consequently, the near-wall gas temperature increases under the 4% wall-attached air fraction. Overall, insufficient wall-attached air provides limited cooling, whereas excessive wall-attached air disturbs the combustion process and weakens the cooling performance. A wall-attached air fraction of 3% therefore provides the best balance between near-wall gas cooling and combustion stability, resulting in the lowest near-wall gas temperature in the rear-wall high-temperature corrosion region.

4.2. Effect of Wall-Attached Air Fraction on Near-Wall Gas Atmosphere Distribution in High-Temperature Corrosion Regions of the Left, Right, and Rear Furnace Walls

4.2.1. CO Concentration Distribution

Figures 14-16 present the height-wise CO concentration distributions near the left furnace wall under different wall-attached air fractions.

Figure 14 presents the height-wise CO concentration distributions near the left furnace wall under wall-attached air fractions of 2%, 3%, and 4%. The CO concentration decreases initially and then increases as the wall-attached air fraction increases. At a wall-attached air fraction of 2%, the wall-attached air supply is insufficient to provide adequate oxygen in the near-wall region. As a result, CO produced during pulverized coal combustion cannot be completely oxidized to CO_2 and accumulates near the furnace wall. Consequently, relatively high CO concentrations are observed in the near-wall region of the high-temperature corrosion area, indicating the presence of a strong reducing atmosphere.

When the wall-attached air fraction is increased to 3%, the additional air improves oxygen availability in the near-wall region and promotes the oxidation of CO to CO_2. At the same time, moderate airflow enhancement improves fuel-air mixing, resulting in more complete combustion and lower CO concentrations.

However, when the wall-attached air fraction is further increased to 4%, the CO concentration increases again. This increase is attributed to the excessive wall-attached air, which alters the original flow field and oxygen distribution. The resulting non-uniform combustion leads to locally fuel-rich regions where CO oxidation is inhibited. Overall, a wall-attached air fraction of 3% provides the best balance between oxygen supply, fuel-air mixing, and combustion stability, resulting in the lowest CO concentration near the left furnace wall.

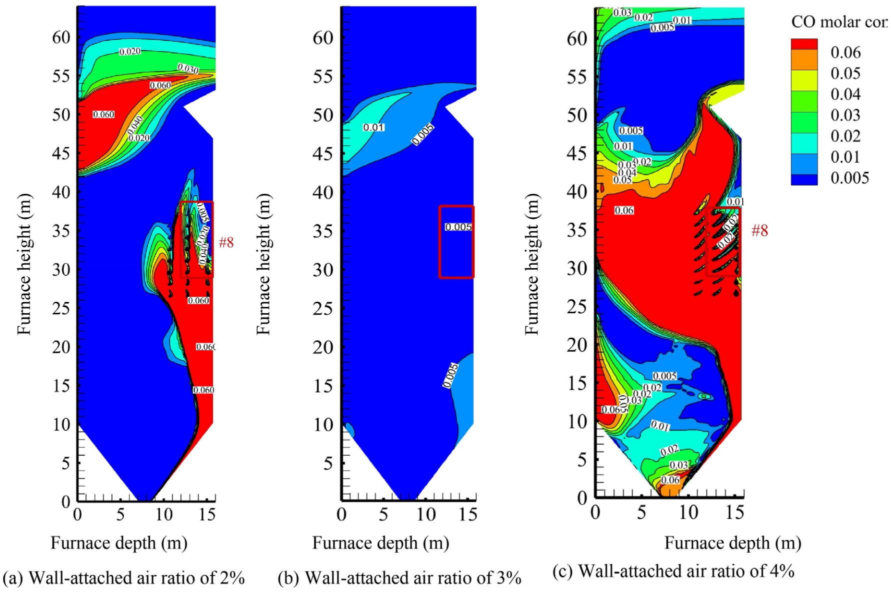

Figure 14. CO concentration distributions on the left walls with different wall-attached air fractions.

Figure 15 presents the height-wise CO concentration distributions near the right furnace wall under different wall-attached air fractions. Similar to the left wall, the lowest CO concentration is obtained at a wall-attached air fraction of 3%, whereas higher CO concentrations are observed under the 2% and 4% conditions. At a wall-attached air fraction of 2%, the CO concentration near corner #5 ranges from 0.005 to 0.020, although the affected region is relatively When the wall-attached air fraction is increased to 3%, the CO concentration in the near-wall region of the high-temperature corrosion area near corner #5 decreases to 0.005 - 0.010, while the affected low-CO region expands. When the wall-attached air fraction is further increased to 4%, the CO concentration rises to 0.005 - 0.060, indicating that excessive wall-attached air weakens the improvement in the near-wall atmosphere.

At a wall-attached air fraction of 2%, the limited wall-attached air supply provides insufficient oxygen in the near-wall region of the right furnace wall. As a result, the oxidation of CO is inhibited, leading to CO accumulation and the formation of a reducing atmosphere. When the wall-attached air fraction is increased to 3%, the additional air improves oxygen availability and enhances fuel-air mixing, thereby promoting the oxidation of CO to CO_2. Consequently, the CO concentration in the near-wall region of the high-temperature corrosion area decreases to 0.005 - 0.010. At the same time, the expansion of the low-CO region indicates more complete combustion near the wall and a weaker reducing atmosphere, demonstrating that the near-wall combustion atmosphere is effectively improved.

However, when the wall-attached air fraction is further increased to 4%, the CO concentration increases again. The corresponding temperature distributions show a noticeable increase in the near-wall gas temperature, suggesting that excessive wall-attached air enhances the overall combustion intensity. In addition, the excessive air supply alters the original flow field and oxygen distribution, resulting in non-uniform combustion near the wall and inhibiting complete CO oxidation. Consequently, the near-wall CO concentration increases despite the higher oxygen input. Overall, a wall-attached air fraction of 3% provides the best balance between oxygen supply, combustion organization, and CO oxidation, resulting in the lowest CO concentration in the near-wall region of the high-temperature corrosion area and a weaker reducing atmosphere near the right furnace wall.

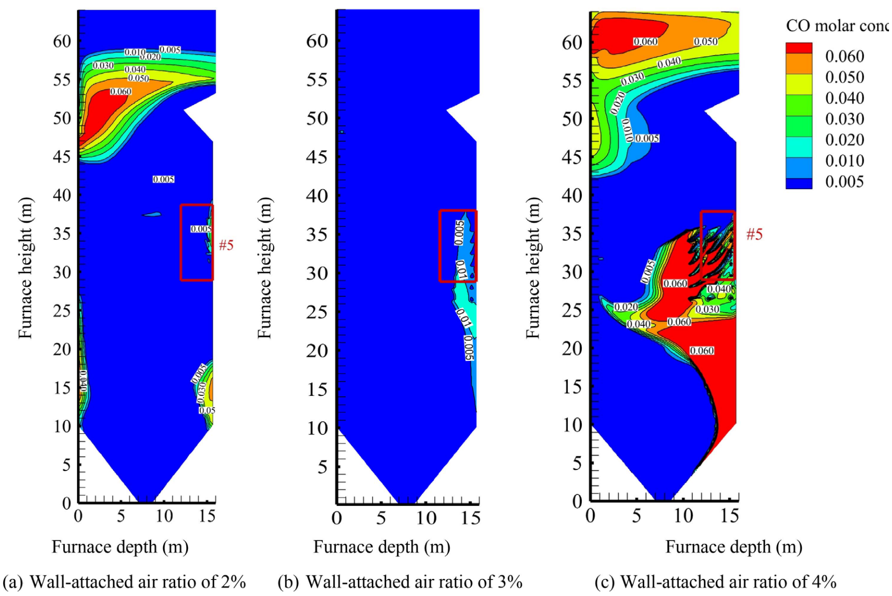

Figure 15. CO concentration distributions on the right walls with different wall-attached air fractions.

Figure 16 presents the height-wise CO concentration distributions near the rear furnace wall under different wall-attached air fractions. The CO concentrations in the #5 and #8 corner regions of the high-temperature corrosion near-wall areas decrease initially and then increase as the wall-attached air fraction increases. At a wall-attached air fraction of 2%, the CO concentration ranges from 0.005 to 0.060 in the high-temperature corrosion near-wall areas around corners #5 and #8. Increasing the wall-attached air fraction to 3% significantly reduces the CO concentration in the near-wall regions, whereas a further increase to 4% causes the CO concentration in the high-temperature corrosion near-wall areas around corners #5 and #8 to rise again to 0.005 - 0.030. At a wall-attached air fraction of 2%, the limited wall-attached air supply provides insufficient oxygen in the near-wall region of the rear wall. As a result, the oxidation of CO to CO_2 is inhibited, leading to relatively high CO concentrations near corners #5 and #8 in the high-temperature corrosion near-wall areas, and the persistence of a strong reducing atmosphere. When the wall-attached air fraction is increased to 3%, the additional air improves oxygen availability and enhances fuel-air mixing near the rear wall, thereby promoting CO oxidation and reducing the CO concentration in the near-wall high-temperature corrosion regions. Consequently, the reducing atmosphere is significantly weakened, providing more favorable conditions for suppressing high-temperature corrosion.

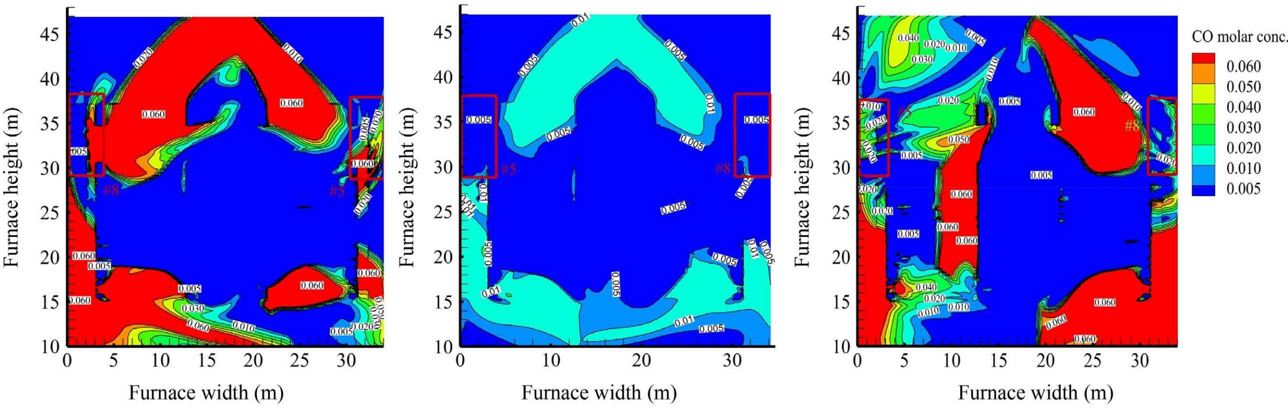

(a) Wall-attached air ratio of 2% (b) Wall-attached air ratio of 3% (c) Wall-attached air ratio of 4%

Figure 16. CO concentration distributions on the rear walls with different wall-attached air fractions.

However, when the wall-attached air fraction is further increased to 4%, the CO concentration increases again, with a maximum value of 0.030. The corresponding temperature distributions show a noticeable increase in near-wall gas temperature, suggesting that excessive wall-attached air enhances the overall combustion intensity. In addition, the excessive air supply alters the original flow field and oxygen distribution near the rear wall, resulting in non-uniform combustion and incomplete CO oxidation in local regions. Consequently, the near-wall CO concentration in the high-temperature corrosion near-wall regions increases despite the higher oxygen input. Overall, a wall-attached air fraction of 3% provides the most effective reduction in the near-wall reducing atmosphere and therefore offers the greatest potential for mitigating high-temperature corrosion of the rear water-cooled wall.

4.2.2. O_2 Concentration Distribution

Figures 17-19 present the height-wise O_2 concentration distributions along the left, right, and rear furnace walls under different wall-attached air fractions.

The introduction of wall-attached air increases the oxygen concentration in the near-wall region by supplying additional secondary air to the high-temperature corrosion-sensitive areas. As the wall-attached air fraction increases, the near-wall

O_2 concentration increases initially and then decreases.

At a wall-attached air fraction of 2%, the limited wall-attached air supply provides insufficient oxygen in the near-wall region. Consequently, relatively low O_2 concentrations are maintained near corners #5 and #8 in the high-temperature corrosion near-wall regions because oxygen is continuously consumed during pulverized coal combustion and CO oxidation. Under this condition, the oxidizing atmosphere remains weak, allowing reducing species to accumulate and increasing the risk of high-temperature corrosion.

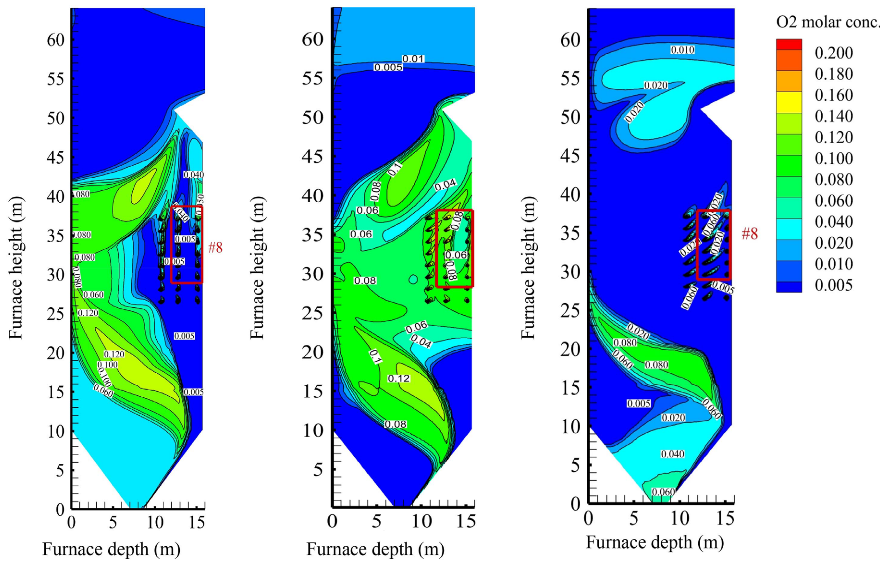

(a) Wall-attached air ratio of 2% (b) Wall-attached air ratio of 3% (c) Wall-attached air ratio of 4%

Figure 17. O_2 concentration distributions on the left walls with different wall-attached air fractions.

When the wall-attached air fraction is increased to 3%, the additional wall-attached air enhances oxygen supply to the near-wall region, resulting in higher O_2 concentrations near corners #5 and #8 in the high-temperature corrosion near-wall regions. Under this condition, the wall-attached air effectively improves oxygen availability without significantly disturbing the original flow field, thereby creating a more favorable atmosphere for mitigating high-temperature corrosion.

However, when the wall-attached air fraction is further increased to 4%, the near-wall O_2 concentration decreases instead of continuing to increase. Excessive wall-attached air alters the original flow field and redistributes the oxygen supply in the furnace. At the same time, the intensified combustion accelerates oxygen consumption, resulting in lower O_2 concentrations near corners #5 and #8 in the high-temperature corrosion near-wall regions despite the higher air supply.

Overall, a wall-attached air fraction of 3% provides the best balance between oxygen supply, combustion stability, and near-wall atmosphere regulation. Under this condition, the highest O_2 concentrations are obtained in the high-temperature corrosion regions of the left, right, and rear furnace walls, providing the most favorable conditions for mitigating high-temperature corrosion.

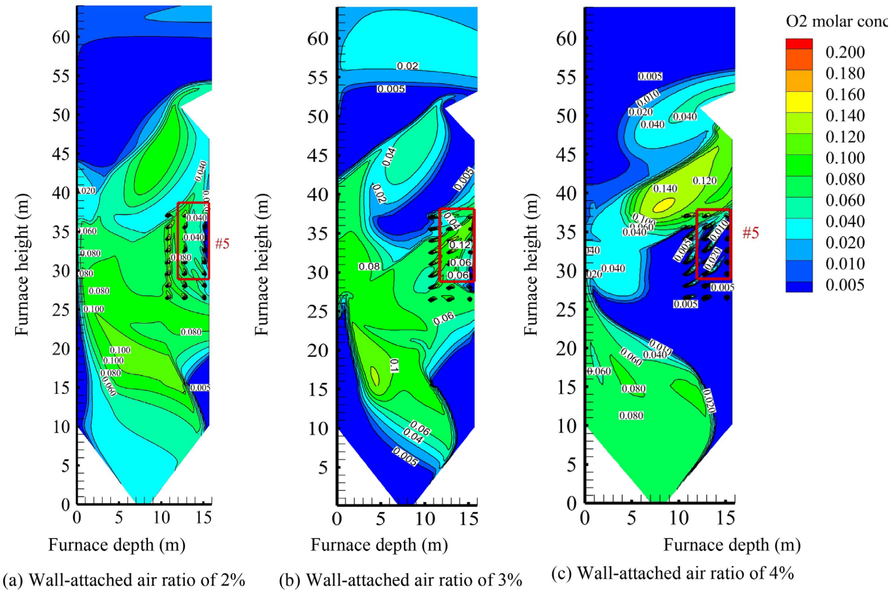

Figure 18. O_2 concentration distributions on the right walls with different wall-attached air fractions.

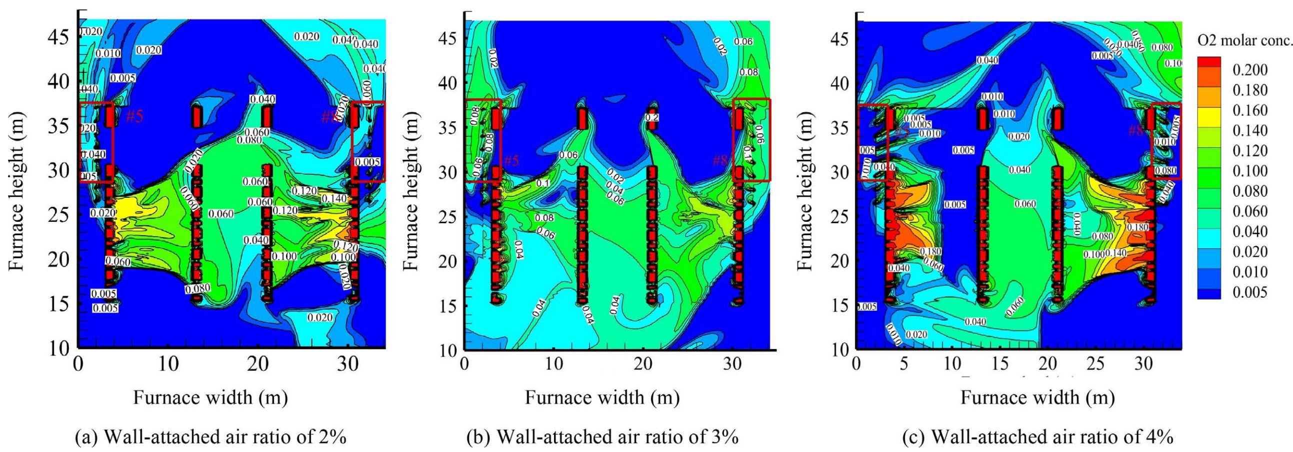

Figure 19. O_2 concentration distributions on the rear walls with different wall-attached air fractions.

4.2.3. Distribution Characteristics of H_2S Concentration

Figures 20-22 present the height-wise H_2S concentration distributions along the left, right, and rear furnace walls under different wall-attached air fractions.

At a wall-attached air fraction of 2%, relatively high H_2S concentrations are observed near corner #8 of the left wall, corner #5 of the right wall, and corners #5 and #8 of the rear wall in the high-temperature corrosion near-wall regions, indicating the presence of a strong sulfur-containing reducing atmosphere in the near-wall region. When the wall-attached air fraction is increased to 3%, the H_2S concentration decreases markedly. The H_2S concentration near corners #5 and #8 is reduced to approximately 50 - 100 ppm, indicating a substantial improvement in the near-wall corrosion environment. However, when the wall-attached air fraction is further increased to 4%, the H_2S concentration rises again, and regions with relatively high H_2S concentrations reappear near corners #5 and #8 in the high-temperature corrosion near-wall regions.

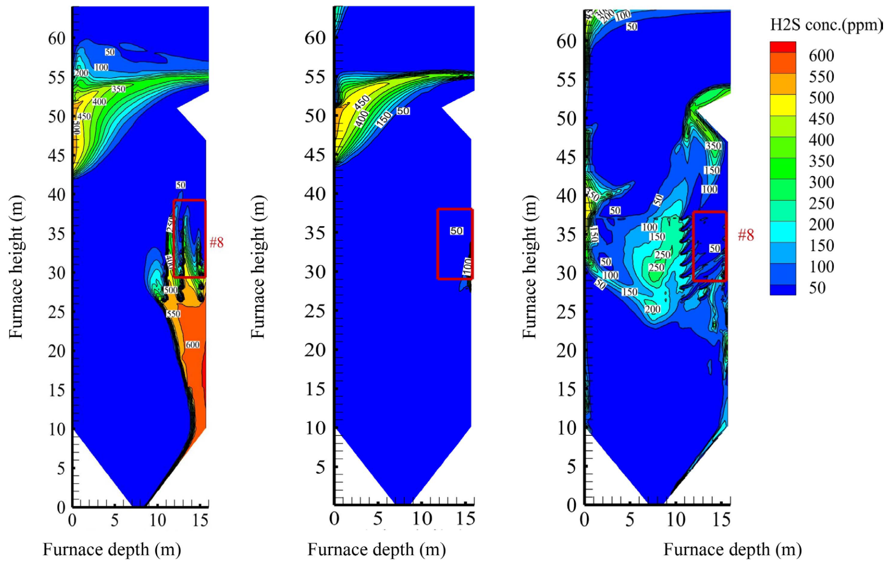

(a) Wall-attached air ratio of 2% (b) Wall-attached air ratio of 3% (c) Wall-attached air ratio of 4%

Figure 20. H_2S concentration distributions on the left walls with different wall-attached air fractions.

At a wall-attached air fraction of 2%, the relatively low wall-attached air supply provides limited improvement in the oxygen environment near the furnace wall, resulting in an oxygen-deficient near-wall region. Under insufficient oxidizing conditions, sulfur-containing reducing species generated during pulverized coal combustion cannot be effectively oxidized, leading to H_2S accumulation near the wall.

When the wall-attached air fraction is increased to 3%, the additional air significantly improves oxygen availability and enhances the oxidizing capacity of the near-wall region, thereby promoting H_2S oxidation and reducing its accumulation. Meanwhile, the wall-attached air strengthens the mixing between the injected air and high-temperature flue gas, further weakening the formation of sulfur-containing reducing gases in the high-temperature corrosion near-wall regions.

However, when the wall-attached air fraction is further increased to 4%, the H_2S concentration increases compared with that at 3%. Combined with the temperature and CO concentration results, excessive wall-attached air modifies the local flow field and oxygen distribution near the wall. The resulting non-uniform combustion environment leads to the reformation of locally reducing regions, where H_2S oxidation is inhibited and H_2S concentration increases in some areas.

Overall, the H_2S concentration distributions under different wall-attached air fractions indicate that a 3% wall-attached air fraction provides the best balance between oxygen supply, combustion organization, and sulfur-containing species oxidation. Under this condition, the lowest H_2S concentrations are obtained in the high-temperature corrosion near-wall regions, resulting in a substantially weakened sulfide corrosion environment in the near-wall region.

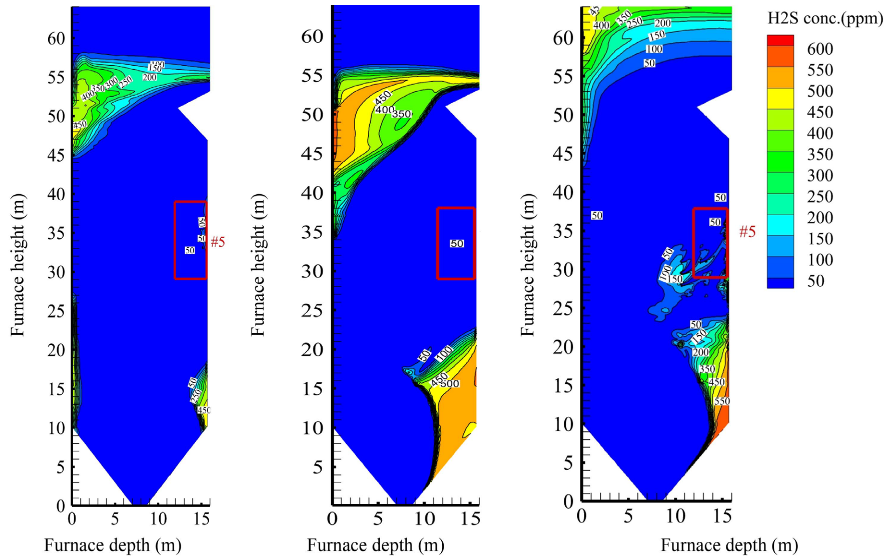

(a) Wall-attached air ratio of 2% (b) Wall-attached air ratio of 3% (c) Wall-attached air ratio of 4%

Figure 21. H_2S concentration distributions on the right walls with different wall-attached air fractions.

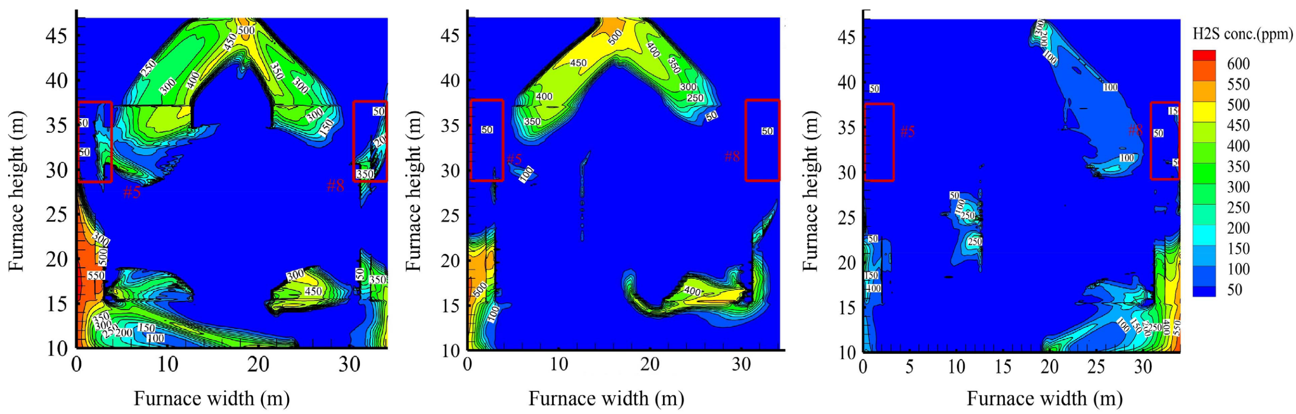

(a) Wall-attached air ratio of 2% (b) Wall-attached air ratio of 3% (c) Wall-attached air ratio of 4%

Figure 22. H_2S concentration distributions on the rear walls with different wall-attached air fractions.

5. Experimental Validation

To evaluate the effectiveness of the wall-attached air retrofit in mitigating high-temperature corrosion on the left, right, and rear water-cooled walls, field measurements of the reducing atmosphere in the burner region are conducted under a stable 1000 MW load and conventional operating conditions. Measurements are performed in the near-wall gas regions adjacent to the left, right, and rear water-cooled walls. In the high-temperature corrosion-sensitive regions near corners #5 and #8, two rows of measurement points are arranged on each side wall, and two rows of measurement points are arranged on the rear wall. The near-wall concentrations of O_2, CO, and H_2S are measured to characterize the combustion atmosphere adjacent to the water-cooled walls.

The aforementioned numerical simulation results have demonstrated the spatial distribution characteristics of near-wall temperature and gas species under the 3% wall-attached air condition. The field test results are further used to verify the improvement trends under actual operating conditions. To validate the optimal wall-attached air fraction determined by the numerical simulations, field measurements are conducted under the 3% wall-attached air condition, corresponding to a wall-attached air flow rate of 100.82 $t \cdot h^{-1}$. The wall-attached air flow rate under this condition is determined according to the designed wall-attached air fraction. The field measurement locations are consistent with the numerical analysis regions and are mainly used to evaluate the improvement of the corrosive atmosphere in the near-wall region after the wall-attached air retrofit.

During actual boiler operation, fluctuations in local gas composition are unavoidable due to variations in coal properties, unit load, and operating conditions. Therefore, the experimental results are mainly used to evaluate the variation characteristics and overall changing trends of the gas compositions in the corrosion-sensitive regions. The near-wall atmosphere measurement results before and after the implementation of wall-attached air are summarized in **Table 5** and **Table 6**, respectively.

Table 5. Near-wall atmosphere measurement results in the burner region before the application of wall-attached air.

Elevation /mm	Flue gas species	Left wall (#8)		Rear wall (#8)	Right wall (#5)		Rear wall (#5)
46,110	O_2/%	19.90	5.71	4.12	/	3.45	1.06
	CO/%	0.01	0.09	0.81	/	0.75	4.01
	H_2S/ppm	0.00	116	750	/	265	940
39,700	O_2/%	2.64	1.14	0.24	4.44	8.92	0.25
	CO/%	0.95	1.01	5.86	0.10	0.02	4.65
	H_2S/ppm	148	301	1220	42	62	793
34,900	O_2/%	2.93	0.59	10.98	4.18	6.81	0.46
	CO/%	0.00	4.00	0.00	0.10	0.31	6.89
	H_2S/ppm	53	705	113	20	275	1090

The experimental results show that after the retrofit, the O_2 concentration at the measurement points ranges from 2.69% to 9.14%, while the CO and H_2S concentrations range from 0.18% to 3.51% and 160 to 518 ppm, respectively. Compared with the pre-retrofit condition, the maximum increase in O_2 concentration is 8.34 percentage points, whereas the maximum reductions in CO and H_2S concentrations reach 6.46 percentage points and 400 ppm, respectively. Compared with the condition without wall-attached air, the maximum increase in O_2 concentration is 5.00 percentage points, accompanied by maximum reductions of

3.83 percentage points in CO and 590 ppm in H_2S.

Overall, the implementation of wall-attached air increases the O_2 concentration and decreases the CO and H_2S concentrations in the near-wall flue gas. These results indicate that the reducing atmosphere in the near-wall gas regions adjacent to the water-cooled walls is weakened and that the local combustion environment is improved after the retrofit.

Table 6. Near-Wall atmosphere measurement results in the burner region after the application of wall-attached air.

Elevation /mm	Flue gas species	Left wall (#8)		Rear wall (#8)	Right wall (#5)		Rear wall (#5)
46,110	O_2/%	19.9	5.79	9.14	/	5.05	3.74
	CO/%	0.01	0.08	0.02	/	0.14	0.18
	H_2S/ppm	0.00	138	160	/	180	258
39,700	O_2/%	4.55	3.45	0.63	7.30	9.17	2.69
	CO/%	0.06	0.04	3.09	0.05	0.08	1.06
	H_2S/ppm	110	156	350	130	125	165
34,900	O_2/%	3.47	2.15	5.87	3.23	17.2	0.73
	CO/%	0.04	0.83	2.03	0.03	0.03	3.51
	H_2S/ppm	60	250	518	20	35	501

The experimental results are basically consistent with the variation trends obtained from the numerical simulation. From the overall variation trend, both the experimental and simulation results show that the O_2 concentration near the wall increases, while the CO and H_2S concentrations decrease, indicating that the numerical model can well reflect the improvement effect of wall-attached air on the near-wall combustion atmosphere. After the application of wall-attached air, the wall-attached airflow forms a stable jet along the water-cooled wall, improving the air supply capacity in the near-wall region and increasing the oxygen potential near the wall. The increase in oxygen concentration promotes the further oxidation of CO, improves the local burnout degree, and weakens the reducing atmosphere near the wall, which can effectively alleviate metal corrosion caused by high-temperature corrosive gases and extend the service life of the furnace wall and water-cooled wall.

6. Conclusions

To address the high-temperature corrosion of water-cooled walls in coal-fired boilers, the effects of the novel wall-attached air technology on the near-wall combustion environment and corrosion mitigation are investigated through a combination of numerical simulations and field tests. The main conclusions are summarized as follows:

1) Numerical simulations are performed under wall-attached air fractions of

2%, 3%, and 4% to investigate the temperature characteristics and the distributions of O_2, CO, and H_2S concentrations near the left, right, and rear furnace walls. The results show that increasing the wall-attached air fraction improves the oxidizing atmosphere near the wall. However, excessive wall-attached air affects the local combustion process. Considering the variations in temperature and gas composition, a wall-attached air fraction of 3% provides the optimal condition, increasing O_2 concentration and reducing CO and H_2S concentrations while maintaining stable furnace combustion.

2) Under the 3% wall-attached air condition, the oxidizing atmosphere near the water-cooled wall is enhanced, while the reducing atmosphere is weakened. Compared with the condition without wall-attached air, the O_2 concentration increases and the CO and H_2S concentrations decrease in the near-wall region, accompanied by a reduction in near-wall gas temperature. The wall-attached air forms a near-wall jet that improves local air supply, strengthens gas mixing, promotes burnout, and reduces the H_2S concentration in the near-wall region, thereby weakening the conditions associated with high-temperature sulfide corrosion.

3) Field tests are conducted under the 3% wall-attached air condition to verify the retrofit performance. After the retrofit, the O_2, CO, and H_2S concentrations in the high-temperature corrosion regions are maintained within the ranges of 2.15% - 19.90%, 0.01% - 3.51%, and 0 - 518 ppm, respectively. Compared with the pre-retrofit condition, the maximum increase in O_2 concentration is 8.34 percentage points, while the maximum reductions in CO and H_2S concentrations are 6.46 percentage points and 400 ppm, respectively. Compared with the condition without wall-attached air, the maximum increase in O_2 concentration is 5.00 percentage points, accompanied by maximum reductions of 3.83 percentage points in CO and 590 ppm in H_2S. The experimental results agree well with the numerical predictions, confirming the reliability of the model and the effectiveness of the optimized 3% wall-attached air condition.

4) The results demonstrate that the wall-attached air technology improves the flow and combustion characteristics in the near-wall region, increases oxygen availability near the water-cooled wall, and weakens the reducing atmosphere while decreasing the near-wall gas temperature. Consequently, the development of high-temperature sulfide corrosion is mitigated. The optimized wall-attached air fraction identified in this study provides a theoretical basis and engineering reference for high-temperature corrosion control and wall-attached air system optimization in large-scale coal-fired boilers.

Funding

This work is supported by the CR Power Theory R&D Program (Grant No. CRP-R&D-LX-2025-031).

Author Contributions

Yong Feng: Writing—original draft, Methodology, Formal analysis, Conceptualization. Zhidong Li: Writing—review & editing, Validation, Investigation. Jiahui Zhao: Writing—review & editing, Visualization, Investigation. Zhenggang Wu: Writing—review & editing, Resources, Project administration. Weiyu Wang: Visualization, Investigation, Conceptualization. Hanlin Li: Writing—review & editing, Validation, Investigation. All authors have read and agreed to the published version of the manuscript.

Conflicts of Interest

The authors declare no conflicts of interest regarding the publication of this paper.

References

[1] Su, K., Ouyang, Z., Wang, H., Zhang, J., Ding, H. and Wang, W. (2024) Experimental Study on Municipal Sludge/Coal Co-Combustion Preheated by Self-Preheating Burner: Self-Preheating Two-Stage Combustion and Nox Emission Characteristics. *Energy*, **290**, Article 130222. https://doi.org/10.1016/j.energy.2023.130222

[2] Wang, W., Zhang, J., Gu, Y., Luo, Q., Zhou, G., Li, A., *et al.* (2024) Recent Progress on Thermal Energy Storage for Coal-Fired Power Plant. *Journal of Thermal Science*, **33**, 2138-2150. https://doi.org/10.1007/s11630-024-2015-z

[3] Ding, N., Duan, J., Xue, S., Zeng, M. and Shen, J. (2015) Overall Review of Peaking Power in China: Status Quo, Barriers and Solutions. *Renewable and Sustainable Energy Reviews*, **42**, 503-516. https://doi.org/10.1016/j.rser.2014.10.041

[4] Wu, C., Wang, C., Hou, Z. and Wang, Z. (2025) Flexible Peak Shaving in Coal-Fired Power Plants: A Comprehensive Review of Current Challenges, Recent Advances, and Future Perspectives. *Energy*, **327**, Article 136446. https://doi.org/10.1016/j.energy.2025.136446

[5] Lakkannavar, V., Yogesha, K.B., Prasad, C.D., Phanden, R.K., G, S. and Prasad, S.C. (2024) Thermal Spray Coatings on High-Temperature Oxidation and Corrosion Applications—A Comprehensive Review. *Results in Surfaces and Interfaces*, **16**, Article 100250. https://doi.org/10.1016/j.rsurfi.2024.100250

[6] Xiong, X., Liu, X., Tan, H. and Deng, S. (2020) Investigation on High Temperature Corrosion of Water-Cooled Wall Tubes at a 300 MW Boiler. *Journal of the Energy Institute*, **93**, 377-386. https://doi.org/10.1016/j.joei.2019.02.003

[7] Chen, T., Yao, L., Liu, J., *et al.* (2015) Numerical Simulation of Wall Air Optimization Scheme for a 660 MW Front-and-Rear Wall Opposed Firing Coal-Fired Boiler. *Proceedings of the CSEE*, **35**, 5265-5271. (In Chinese)

[8] Zhang, Z., Luo, Z., Zhong, J., Zheng, L. and Chai, J. (2026) Application of Computer Vision Big Data Algorithms in Accurate Detection of Corrosion Images of Boiler Water-Cooled Wall Tubes. *Procedia Computer Science*, **281**, 207-215. https://doi.org/10.1016/j.procs.2026.04.209

[9] Yao, J., Zhong, X., Zhang, Z., Fan, Z., Hu, J. and Wang, J. (2024) The Fitness and Corrosion Mechanisms of High-Strength Steel in Corrosive Oil-Water Environment at High Temperature. *Materials and Corrosion*, **75**, 247-265. https://doi.org/10.1002/maco.202313912

[10] Yang, X., Liao, Y., Wang, Y., Chen, X. and Ma, X. (2022) Research of Coupling Technologies on Nox Reduction in a Municipal Solid Waste Incinerator. *Fuel*, **314**, Article 122769. https://doi.org/10.1016/j.fuel.2021.122769

[11] Zhong, Y., Wang, X., Xu, G., Ning, X., Zhou, L., Tang, W., *et al.* (2023) Investigation

on Slagging and High-Temperature Corrosion Prevention and Control of a 1000 MW Ultra Supercritical Double Tangentially Fired Boiler. *Energy*, **275**, Article 127455. https://doi.org/10.1016/j.energy.2023.127455

[12] Liu, J., Feng, L., Wu, Y., Feng, R., Chen, S. and Zhao, D. (2024) Numerical Investigation on H_2S Formation in a Pulverized Coal-Fired Boiler Using Recycled Flue Gas as Near-Wall Air. *Energy*, **313**, Article 134134. https://doi.org/10.1016/j.energy.2024.134134

[13] Xu, L., Huang, Y., Zou, L., Yue, J., Wang, J., Liu, C., *et al.* (2019) Experimental Research of Mitigation Strategy for High-Temperature Corrosion of Waterwall Fireside in a 630 Mwe Tangentially Fired Utility Boiler Based on Combustion Adjustments. *Fuel Processing Technology*, **188**, 1-15. https://doi.org/10.1016/j.fuproc.2019.02.001

[14] Yang, W., You, R., Wang, Z., Zhang, H., Zhou, Z., Zhou, J., *et al.* (2017) Effects of Near-Wall Air Application in a Pulverized-Coal 300 MW_e Utility Boiler on Combustion and Corrosive Gases. *Energy & Fuels*, **31**, 10075-10081. https://doi.org/10.1021/acs.energyfuels.7b01476

[15] Khantisopon, K., Singh, S., Jitputti, J., Berndt, C.C. and Ang, A.S.M. (2024) High Temperature Corrosion Resistant and Anti-Slagging Coatings for Boilers: A Review. *High Temperature Corrosion of Materials*, **101**, 1-55. https://doi.org/10.1007/s11085-024-10251-0

[16] Huang, C., Wan, Q., Bei, L., Yang, W., Wang, B., Xu, L., *et al.* (2026) The Impact of Near-Wall Air on Pollutant Emissions and High-Temperature Corrosion in Opposed-Fired Boilers. *Applied Thermal Engineering*, **290**, Article 130022. https://doi.org/10.1016/j.applthermaleng.2026.130022

[17] Jin, Q., Dai, G., Wang, Y., Wang, Z., Shan, Z., Wang, X., *et al.* (2020) High-Temperature Corrosion of Water-Wall Tubes in Oxy-Combustion Atmosphere. *Journal of the Energy Institute*, **93**, 1305-1312. https://doi.org/10.1016/j.joei.2019.11.013

[18] Ning, X., Wang, J., Huang, J., Ding, H., Li, B., Deng, L., *et al.* (2024) Study on High-temperature Corrosion in a 600 MW Opposed Firing Boiler. *Asia-Pacific Journal of Chemical Engineering*, **19**, e3011. https://doi.org/10.1002/apj.3011

[19] Liu, H., Hu, S., Zhang, L., Li, Q., Deng, L. and Che, D. (2019) Influence of Near-Wall Air Position on the High-Temperature Corrosion and Combustion in a 1000 MWth Opposed Wall-Fired Boiler. *Fuel*, **257**, Article 115983. https://doi.org/10.1016/j.fuel.2019.115983

[20] Liu, J., Gu, Y., Feng, L. and Yang, D. (2026) Prediction and Mitigation of H_2S-Induced High-Temperature Corrosion in a 660 MW Boiler Water-Wall. *Materials*, **19**, Article 2074. https://doi.org/10.3390/ma19102074

[21] Wang, X.Y., Huang, Y.J., Xu, L.G., *et al.* (2022) Numerical Simulation on Mitigating High Temperature Corrosion in a Double Tangential Firing Boiler by Adjusting Secondary Air of the Same Layer. *Chemical Industry and Engineering Progress*, **41**, 2292-2300. (In Chinese)

[22] Yue, J.F. and Huang, Y.J. (2024) Analysis and Prevention of High Temperature Corrosion on Water Walls of a 1000 MW Ultra-Supercritical Double Tangential π-Type Pulverized Coal Boiler. *Journal of Energy Research and Utilization*, No. 3, 35-39. (In Chinese)

[23] Lv, Y.X., Zhao, Y.Y., Cao, L.T., *et al.* (2023) Numerical Simulation Study on Preventing High Temperature Corrosion of Water Walls in a Double Furnace Double Tangential Utility Boiler. *Journal of Northeast Electric Power University*, **43**, 39-44. (In Chinese)

[24] Liu, Z.X., Yang, H.L., Zhu, J.Y., *et al.* (2025) Experimental Study on the Control of

High Temperature Sulfur Corrosion in a 600 MW Opposed Wall-Fired Boiler. *Power System Engineering*, **41**, 42-44. (In Chinese)

[25] Cui, Q., Zhang, Z.L. and Li, H.R. (2023) Experimental Study on Preventing High Temperature Corrosion in a 670 MW Opposed Wall Swirl Combustion Boiler. *Journal of Engineering for Thermal Energy and Power*, **38**, 182-188. (In Chinese)

[26] Chen, Q.G., Lin, M.C., Xiang, Q.Y., *et al.* (2022) Numerical Simulation and Engineering Verification of Close-Coupled Overfire Air System in an Ultra-Supercritical Unit Boiler. *Journal of Engineering for Thermal Energy and Power*, **37**, 112-121. (In Chinese)

[27] Qiu, B., Lin, M.C., Zhang, H.D., *et al.* (2021) Research on the Retrofit Technology of High-Speed Close-Coupled Overfire Air in a 660 MW Ultra-Supercritical Boiler. *Energy Engineering*, No. 2, 61-65. (In Chinese)

[28] Shih, T.H., Liou, W.W., Shabbir, A., Yang, Z. and Zhu, J. (1995) A New K-E Eddy Viscosity Model for High Reynolds Number Turbulent Flows. *Computers & Fluids*, **24**, 227-238. https://doi.org/10.1016/0045-7930(94)00032-t

[29] Gosman, A.D. and loannides, E. (1983) Aspects of Computer Simulation of Liquid-Fueled Combustors. *Journal of Energy*, **7**, 482-490. https://doi.org/10.2514/3.62687

[30] Chalhoub, E.S. (2003) Discrete-Ordinates Solution for Radiative-Transfer Problems. *Journal of Quantitative Spectroscopy and Radiative Transfer*, **76**, 193-206. https://doi.org/10.1016/s0022-4073(02)00053-5

[31] Kobayashi, H., Howard, J.B. and Sarofim, A.F. (1977) Coal Devolatilization at High Temperatures. *Symposium* (*International*) *on Combustion*, **16**, 411-425. https://doi.org/10.1016/s0082-0784(77)80341-x

[32] Magnussen, B.F. and Hjertager, B.H. (1977) On Mathematical Modeling of Turbulent Combustion with Special Emphasis on Soot Formation and Combustion. *Symposium* (*International*) *on Combustion*, **16**, 719-729. https://doi.org/10.1016/s0082-0784(77)80366-4

[33] Field, M.A. (1969) Rate of Combustion of Size-Graded Fractions of Char from a Low-Rank Coal between 1200˚K and 2000˚K. *Combustion and Flame*, **13**, 237-252. https://doi.org/10.1016/0010-2180(69)90002-9